KTH ROYAL INSTITUTE
OF TECHNOLOGY

Doctoral Thesis in Civil and Architectural Engineering

Advances in Ventilation Heat Recovery

An assessment of peak load shaving using renewables

BEHROUZ NOUROZI

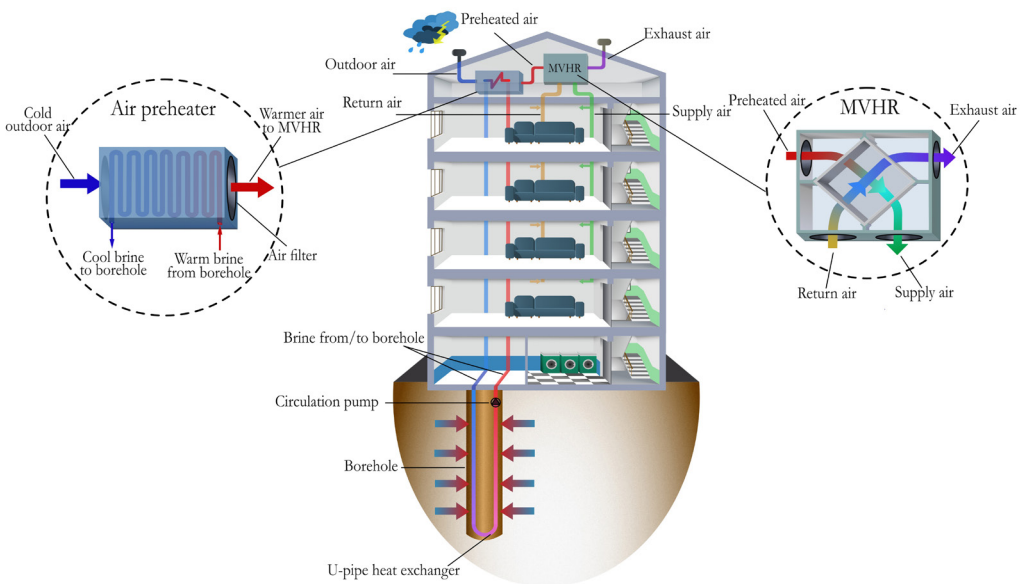

Stockholm, Sweden 2022

Advances in Ventilation Heat Recovery

An assessment of peak load shaving using renewables

BEHROUZ NOUROZI

Academic Dissertation which, with due permission of the KTH Royal Institute of Technology, is submitted for public defence for the Degree of Doctor of Philosophy on Wednesday the 25th May 2022, at 13:00 in B1, Brinellvägen 23, Stockholm.

Doctoral Thesis in Civil and Architectural Engineering
KTH Royal Institute of Technology
Stockholm, Sweden 2022

ISBN 978-91-8040-199-9
TRITA-ABE-DLT-2210

Printed by: Universitetsservice US-AB, Sweden 2022

Abstract

The building sector accounts for approximately 40% of total global energy usage. In residential buildings located in cold climate countries, 30-60% of this energy is used for space heating, 20–30% is lost by discarded residential wastewater, and the rest is devoted to ventilation heat loss.

Sweden experienced a construction boom during the so-called Million Programme (MP) in the 1960s and 1970s. A retrofit requirement of buildings constructed during this era shifted from pure exhaust ventilation to mechanical ventilation with heat recovery (MVHR), which peaked in Swedish dwellings between 1990 and 2000. It is estimated that 43% of Swedish multi-family buildings built during this decade were equipped with MVHR systems. A common problem with efficient MVHR systems is frost formation during cold winter hours when cold outdoor air and humid, warm return air exchange heat in the air handling unit. Outdoor air preheating using locally available renewable heat sources has been an alternative solution to prevent frost formation in the heat exchanger.

The main objective of this work was to investigate the solutions for improving the performance of MVHR systems during the coldest periods of the year. The primary focus was frosting, a critical problem in MVHR units that operate during cold periods. The recovered heat from discarded wastewater and the local geothermal energy were the two investigated renewable heat sources used to preheat the incoming cold outdoor air to the MVHR in order to prevent frost formation on the heat exchanger surface.

The performance of the suggested outdoor air preheating systems and the impact of air preheating on the entire system's thermal efficiency were evaluated by TRNSYS dynamic simulations. Temperature control systems were proposed based on the identified frost thresholds to efficiently use the limited thermal capacity of wastewater and maintain a high heat recovery of MVHR. Two outdoor air preheating systems configurations with temperature-stratified and -unstratified tanks were designed and compared. A life cycle cost analysis was applied to further investigate the cost-effectiveness of the studied systems.

Detailed heat transfer simulation of the ventilation heat exchanger revealed that when condensation occurred in the heat exchanger, the heat transfer rate between the return airflow and the plate increased significantly. This was reflected by a sharp increase in the plate temperature, increasing the supply air temperature to the building. Monitoring the relative humidity of the airflow at the inlet of the heat exchanger and using the onset values of frosting/condensation suggested in

this work will allow a more precise and proactive prediction of freezing and more efficient utilization of outdoor air preheating resources.

The results obtained from the simulation of building energy usage indicated that residential wastewater had sufficient thermal potential to reduce the defrosting need for MVHR systems (equipped with a plate heat exchanger) in central Swedish cities to 25%. For colder regions in northern Sweden, the defrosting time was decreased by 50%. The suggested temperature control systems ensured high MVHR temperature efficiencies above 80% for most of the heating season, while the frosting period was minimized. LCC analysis revealed that outdoor air preheating systems equipped with temperature stratified wastewater tank and an unstratified storage tank could pay off their investment costs in 17 and 8 years, respectively.

Keywords: Peak heat load shaving; renewable energy; ventilation heat recovery; frosting in heat exchangers; Heat transfer

Sammanfattning

Byggsektorn står för cirka 40% av den totala globala energianvändningen. I bostadshus belägna i länder med kallt klimat används 30–60% av denna energi för uppvärmning av rum, 20–30% går förlorat i utgående avloppsvatten och resten är ventilationsvärmeförluster.

Sverige upplevde en byggboom under det så kallade miljonprogrammet (MP) på 1960- och 1970-talen. Byggnader från denna tid har haft behov av renovering från ren frånluftsventilation till mekanisk ventilation med värmeåtervinning (FTX). Omställningen nådde sin topp mellan 1990 och 2000. Uppskattningsvis 43% av svenska flerfamiljshus byggda under detta decennium utrustade med FTX-system. Ett vanligt problem med effektiva FTX-system är frostbildning under kalla vintertimmar när kall uteluft och fuktig, varm returluft har värmeutbyte i aggregatet. Förvärmning av uteluft med lokalt tillgängliga förnybara värmekällor har varit en lösning för att förhindra frostbildning i värmeväxlaren.

Huvudsyftet med detta arbete var att undersöka lösningar som förbättrar prestandan hos FTX-system under årets kallaste perioder. Det primära fokuset var frostbildning, ett kritiskt problem i MVHR-enheter som är i drift under kalla perioder. I denna undersökning var återvunnen värme ur utgående avloppsvatten och lokal geotermisk energi två förnybara värmekällorna som användes för att förvärma den inkommande kalla utomhusluften till FTX-systemet. Detta för att förhindra frostbildning på värmeväxlarens ytor.

Prestandan hos föreslagna förvärmningssystem för inkommande utomhusluft liksom luftförvärmningens inverkan på hela termiska systemeffektiviteten utvärderades med dynamiska simuleringar i TRNSYS. Temperaturkontrollsystem, baserade på identifierade trösklar för frostbildning, föreslogs för att effektivt kunna nyttja det begränsade termiska energiinnehållet i avloppsvattnet och få hög värmeåtervinning med FTX. Två konfigurationer för förvärmning av utomhusluft med temperaturskiktade respektive oskiktade tankar skapades och jämfördes. Livscykelkostnadsanalys användes för att ytterligare undersöka kostnadseffektiviteten hos de studerade systemen.

Detaljerad simulering av värmeöverföring i ventilationsvärmeväxlare visade att när kondens uppstod i värmeväxlaren ökade värmeöverföringen mellan returluftflödet och plattan avsevärt. Detta resulterade i kraftig ökning av platttemperaturen och ökade tilluftstemperaturen till byggnaden. Övervakning av relativa luftfuktigheten i luftflödet vid värmeväxlarens inlopp och användning av i detta arbete föreslagna startvärdena för frostbildning/kondensering, kommer att möjliggöra en

noggrannare proaktiv förutsägelse av tillfrysningen. Det innebär också effektivare utnyttjande av utomhusluftens potential för förvärmning.

Resultaten från simuleringar av byggnaders energianvändning visade att avloppsvatten från bostäder har termisk potential att minska avfrostningsbehovet. Med FTX-system och plattvärmeväxlare i mellersta Sverige kunde avfrostningsbehovet i vissa fall minska till 25%. För kallare regioner i norra Sverige minskade avfrostningstiden med 50%. De föreslagna temperaturkontrollsystemen säkerställde hög FTX-temperatureffektivitet, dvs. över 80% under större delen av uppvärmningssäsongen, samtidigt som perioden för frostbildning minimerades. LCC-analys visade att förvärmningssystem för utomhusluft utrustade med temperaturskiktad avloppsvattentank, alternativt oskiktad lagringstank kunde betala av sina investeringskostnader på 17 respektive 8 år.

Nyckelord: förnybar energi; ventilation värmeåtervinning; frosting i värmeväxlare; värmeöverföring

Preface

Five years have passed since I started my journey as a PhD candidate, and I have spent every day ever since with many wonderful people who left a permanent mark on my life. First and foremost, I would like to thank my main supervisor Prof. Sasan Sadrizadeh for his keen support and encouragement. I have learned A LOT from you, and I enjoyed every single moment we spent traveling together over the world.

I want to thank Dr. Adnan Ploskić, not only as my supervisor and project leader but also as a dear friend, for giving me space to take the responsibility of undertaking this path and grow independently. Our timely discussions were always a source of inspiration and an energy booster when I felt overwhelmed with the workload. I am also grateful to Dr. Qian Wang for his firm support and friendship during this period, especially the continuation of my research after my Licentiate. I am also thankful to Prof. Sture Holmberg for acting as my principal supervisor during my licentiate studies. I was lucky to have the opportunity to utilize his knowledge and expertise.

I would also like to thank my colleagues and friends at the Department of Civil and Architectural Engineering at KTH for making these years memorable and full of fun. Special thanks to Assoc. Prof. Yuxiang Chen for hosting me as a visiting researcher at the University of Alberta during Jan-May 2020. Much appreciation and love go to my friends outside KTH, who made Stockholm a second home for me.

This PhD work was financially supported by the Swedish Energy Agency, SBUF (Development Fund of Swedish Construction Industry), and Boverket (the Swedish National Board of Housing, Building and Planning). Contributions from our industrial partners, Skanska AB, Swegon AB, Incoord Installations Coordinator AB, Energiverket AB, ÖrebroBostäder AB, SKB Stockholms Kooperativa Bostadsförening AB, Riksbyggen, and Stockholmshem are acknowledged.

Finally, I express innumerable thanks to my mother and siblings for their endless love, support, and encouragement. I was the most fortunate to have your passion along this arduous journey.

Stockholm, May 2022
Behrouz Nourozi

Publications

This doctoral thesis is based on the outcomes presented in the following scientific papers appended at the end of the text, labelled **Paper 1**–**7**.

Paper 1 **Behrouz Nourozi**, Qian Wang, Adnan Ploskić "Energy and defrosting contributions of preheating cold supply air in buildings with balanced ventilation". *Journal of Applied Thermal Engineering* 146 (2019) 180-189.

Paper 2 **Behrouz Nourozi**, Qian Wang, Adnan Ploskić "Maximizing thermal performance of building ventilation using geothermal and wastewater heat". *Journal of Resources, Conservation and Recycling* 143 (2019) 90-98.

Paper 3 **Behrouz Nourozi**, Sasan Sadrizadeh, Adnan Ploskić "Critical values for condensation and frost onset in air recuperators – A detailed heat transfer evaluation". *Journal of Applied Thermal Engineering* (Under review) April 2022.

Paper 4 **Behrouz Nourozi**, Adnan Ploskić, Yuxiang Chen, Justin Ning-Wei Chiu, Qian Wang "Heat transfer model for energy-active windows – An evaluation of efficient reuse of waste heat in buildings". *Journal of Renewable Energy* 162 (2020): 2318-2329.

Paper 5 **Behrouz Nourozi**, Qian Wang, Adnan Ploskić "Identifying frost threshold in a balanced mechanical ventilation system by inlet and exhaust air temperature control". Proceedings of *The 11th International Symposium on Heating, Ventilation and Air Conditioning (ISHVAC)* 12-15 July 2019, Harbin, China.

Paper 6 **Behrouz Nourozi**, Qian Wang, Adnan Ploskić "Preheating cold supply air to mechanical balanced ventilation using wastewater or passive geothermal energy". Proceedings of *The 16th International Building Performance Simulation Association (IBPSA)* 2-4 September 2019, Rome, Italy.

Paper 7 Simon Härer, **Behrouz Nourozi**, Qian Wang, Adnan Ploskić "Frost reduction in mechanical balanced ventilation by efficient means of preheating cold supply air. Proceedings of *The 10th International Conference on Indoor Air Quality, Ventilation and Energy Conservation in Buildings (IAQVEC)* 5-7 September 2019, Bari, Italy.

Papers **1**–**6** were planned, implemented and written by Behrouz Nourozi. The co-authors contributed to the papers with comments and supervision. Paper **7** was the outcome of a bachelor thesis work supervised by Behrouz Nourozi who also contributed to the writing and visualization.

In addition to the abovementioned papers, the author has contributed to the following related publications that are not included in the thesis:

Journal articles:

Paper 8 Lars Herre, **Behrouz Nourozi**, Mohammad Reza Hesamzadeh, Qian Wang, Lennart Söder. "Provision of Multiple Services with Controllable Loads as Multi-Area Thermal Energy Storage". *Journal of Energy Storage* (2022) (Under review).

Paper 9 Henrikki Pieskä, Cong Wang, **Behrouz Nourozi**, Adnan Ploskić, Qian Wang. "Holistic performance evaluation of novel high-temperature cooling systems supplied by geothermal energy in the Mediterranean climate". *Journal of Building Engineering* (2022) (Under review).

Paper 10 **Behrouz Nourozi**, Sture Holmberg, Christophe Duwig, Pawel Wargocki, Sasan Sadrizadeh. "Heating energy implications of utilizing gas-phase air cleaners in buildings' centralized air handling units". *Journal of Energy and Buildings* (2022) (Under review).

Paper 11 Trond Thorgeir Harsem, **Behrouz Nourozi**, Amirmohammad Behzadi, Sasan Sadrizadeh. "Design and Parametric Investigation of an efficient heating system, an effort to obtain a higher seasonal performance factor". *Journal of Energies* (2021) 14, 8475.

Paper 12 Cong Wang, Qian Wang, **Behrouz Nourozi**, Henrikki Pieskä, Adnan Ploskić. "Evaluating the cooling potential of a geothermal-assisted ventilation system for multi-family dwellings in the Scandinavian climate". *Journal of Building and Environment* 204 (2021): 108114.

Paper 13 **Behrouz Nourozi**, Simon Härer, Qian Wang, Adnan Ploskić. "Life cycle cost analysis of air preheating systems using wastewater and geothermal energy". *The REHVA European HVAC Journal* 56 (1) (2019) 47-51.

Conference proceedings:

Paper 14 Narges Hassani Pour Mahani, **Behrouz Nourozi**, Sasan Sadrizadeh, Omid Abouali. "Thermal comfort analysis in office rooms served by low-temperature heating systems. Proceedings of *The 17th International Conference of of the International Society of Indoor Air Quality & Climate (Indoor Air)* 12-16 June 2022, Kuopio, Finland.

Paper 15 **Behrouz Nourozi**, Sasan Sadrizadeh, Adnan Ploskić. "Condensation and Frost Onset of Air-to-Air Heat Exchangers – A Detailed Heat Transfer Analysis. Proceedings of *The 5th International Conference on Building Energy and Environment (COBEE)* 25-29 July 2022, Montreal, Canada.

Paper 16 Amirmohammad Behzadi, **Behrouz Nourozi**, Sasan Sadrizadeh. "Techno-environmental assessment of a green and efficient concept based on smart thermal storage interacted with low-temperature heating and high-temperature. Proceedings of *The 5th International Conference on Building Energy and Environment (COBEE)* 25-29 July 2022, Montreal, Canada.

Paper 17 Amirmohammad Behzadi, **Behrouz Nourozi**, Sasan Sadrizadeh. "Proposal and analysis of a geothermal-assisted low-temperature heating and high-temperature cooling system. Proceedings of *The European Geothermal Congress (EGC)* 17-21 October 2022, Berlin, Germany.

Paper 18 **Behrouz Nourozi**, Ida Iranmanesh, Sture Holmberg, Christophe Duwig, Emil Andersson, Alireza Afshari, Samira Rahnama, Per Erik Nilsson, Omid Abouali, Trond Thorgeir Harsem, Adnan Ploskic, Sasan Sadrizadeh. "Review of air cleaning technologies for energy-efficient ventilation. Proceedings of *The Healthy Buildings 2021-America Conference* 18-20 January 2022, Hawaii, USA.

Paper 19 Trond Thorgeir Harsem, **Behrouz Nourozi**, Frida Heggebø, Maria Olsen Wulff, Parastoo Sadeghian, Hans Martin Mathisen, Guangyu Cao, Sasan Sadrizadeh. "Development of an Extended Reality Technology to combat surgical site infections. Proceedings of *The Healthy Buildings 2021-America Conference* 18-20 January 2022, Hawaii, USA.

Paper 20 **Behrouz Nourozi**, Adnan Ploskić, Yuxiang Chen, Justin Ning-Wei Chiu, Qian Wang. "Integrated Energy Active Windows with Low-Temperature Heating Systems in Cold Climates. Proceedings of *The 16th International Conference of of the International Society of Indoor Air Quality & Climate (Indoor Air)* 1-5 November 2020, Seoul, South Korea.

Paper 21 Anni Wei, **Behrouz Nourozi**, Yuxiang Chen. "Incorporating Plants Modelling in Greenhouse Design. Proceedings of *The International Building Performance Simulation Association IPBSA-Canada eSim2020* 14-16 June 2021, Vancouver, Canada.

Paper 22 **Behrouz Nourozi**, Qian Wang, Adnan Ploskić. "An efficient heat recovery system in Swedish low-energy multi-family buildings. Proceedings of *The International Conference on Resource Sustainability (iCRS)* 27-29 June 2018, Beijing, China.

Thesis:

Lic. thesis **Behrouz Nourozi** "Sustainable building ventilation solutions with heat recovery from waste heat. *KTH Royal Institute of Technology* Licentiate dissertation 2019.

Nomenclature

Abbreviations

ACH	Air change rate per hour
AHU	Air handling unit
AP	Air preheater
BBR	Swedish building regulations
DH	District heating
DHW	Domestic hot water
EAW	Energy active window
HX	Heat exchanger
IAQ	Indoor air quality
LCC	Life cycle cost
MVHR	Mechanical ventilation with heat recovery
NPV	Net present value
RH	Relative humidity
SEE	Standard error of estimate
TGW	Triple glazed window
WW	Wastewater

Latin Symbols

$c_{p,air}$	Air specific heat capacity	$J/kg°C$
$c_{p,ww}$	Wastewater specific heat capacity	$J/kg°C$
d_s	Slot width	m
D_h	Hydraulic diameter	m
G	Mass velocity	kg/m^2s
h	Heat transfer coefficient	$W/m^2°C$
k	Thermal conductivity	$W/m°C$
m_{air}	Ventilation air mass	kg
$\dot{m}_{air}$	Ventilation mass flow rate	kg/s
$\dot{m}_{ww}$	Wastewater mass flow rate	kg/s
P_w	Available thermal power in brine/wastewater	W
Q	Recovered heat (from ventilation and wastewater)	W
Nu	Nusselt number	$-$
Pr	Prandtl number	$-$
Re	Reynolds number	$-$
Ri	Richardson number	$-$
T	Temperature	$°C$
U	Thermal transmittance (of window)	$W/m^2°C$

Greek Symbols

η_{MVHR}	Temperature efficiency of MVHR	%
ρ	Density	kg/m^3
ν	Kinematic viscosity	m^2/s
μ	Dynamic viscosity	kg/ms
$\Delta\theta_{air}$	Reduction in ventilation air temperature	$^\circ C$
$\Delta\theta_{ww}$	Reduction in wastewater temperature	$^\circ C$
Δx	Grid size	$-$
Δh_v	Specific enthalpy of vaporization	J/kg

Subscripts

$cond$	Conduction
$conv$	Convection
dp	Dew point
exh	Exhaust
in	Inlet
i	Denoting a term in a sequence along the height
j	Denoting a term in a sequence along the cross-section
p	Plate
pre	Preheated
rad	Radiation
ret	Return
sat	Saturation
$surf$	Surface

Contents

Chapter 1

Introduction

The ever-increasing dependency of human beings and our society on energy is inevitable. The scarcity of non-renewable energy resources, the devastating impacts of using traditional energy sources, and their sky-rocketing prices are among the factors that have mandated significant and continual revision in minimum energy performance requirements of different sectors. The expanding residential and service sector is currently responsible for approximately 40% of the total energy usage, 90% of which is attributed to households and non-residential buildings (Swedish Energy Agency, 2017). Following the directive 2009/28/EC of the European Parliament, two amended directives, 2018/2001 and 2018/2002 of the European Parliament and of the Council of 11 December 2018 on "the promotion of the use of energy from renewable sources" and "energy use" were released, respectively (EU Directive 2018/2001, 2018; EU Directive 2018/2002, 2018). The directives established a set of binding measures as the 2030 perspective to cut greenhouse gas emissions by 40% and increase energy efficiency by 40% relative to 1990 levels.

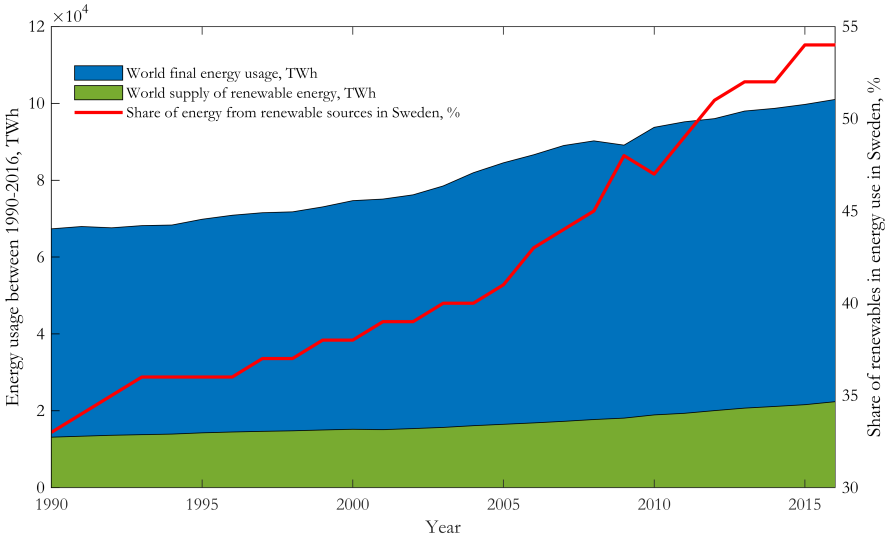

Figure 1.1: Share of renewables in total energy usage (Grahn, 2019)

Figure 1.1 shows how the share of renewable energy sources has increased from 1.31×104 TWh in 1990 to 2.34×104 TWh in 2016 (from 19% to 22% of the total energy use). However, the share of renewables in Sweden has been more than the global average; it was augmented to more than 54% of total energy usage in Sweden in 2016.

a) Share of heating energy providers to apartment buildings

b) Required heating energy based on building types

Figure 1.2: Total energy usage for heating and DHW in 2016 (Statens Energimyndighet, 2016)

Heat recovery from waste heat in residential buildings can increase the overall energy efficiency of this sector. The comfortable room temperature in Swedish residential buildings is 20°C, and the outgoing wastewater has an average temperature of 20°C (varies between 19°C–25°C). Using heat recovery technologies for both sources, the outgoing wastewater and air temperature can be reduced to 5°C. Assuming daily water usage of 160 l/person and 1000 kg/person of ventilation, air for the whole population can reveal the potential of the total waste heat by wastewater and ventilation in the entire country; see Equation 1.1.

$$Q = (\dot{m}_{air} c_p, air \Delta\theta_{air} + \dot{m}_{ww} c_p, ww \Delta\theta_{ww}) \times population \approx 70^{GWh}/_{\text{day}} \\ = 25^{TWh}/_{year} \quad (1.1)$$

The wasted heat energy from both ventilation air and wastewater in residential

buildings in Sweden is approximately equal to the required annual energy for heating and DHW for multi-family buildings, as depicted in Figure 1.2. The intention to further use renewables has triggered the idea of recovering the waste heat from buildings and reusing it to improve buildings' energy performance.

1.1 Research motivation

In Sweden, the peak heating demand load occurs from November to February; see Figure 1.3. Due to high power demand in this period, fossil fuels are used during the coldest periods to meet the market requirements. This period is also associated with the highest CO2 emission and production costs Levin and Karlsson (2015). Therefore, this stipulates an attempt to reduce the energy usage (kWh) and both electrical and thermal peak loads (kW) in this period.

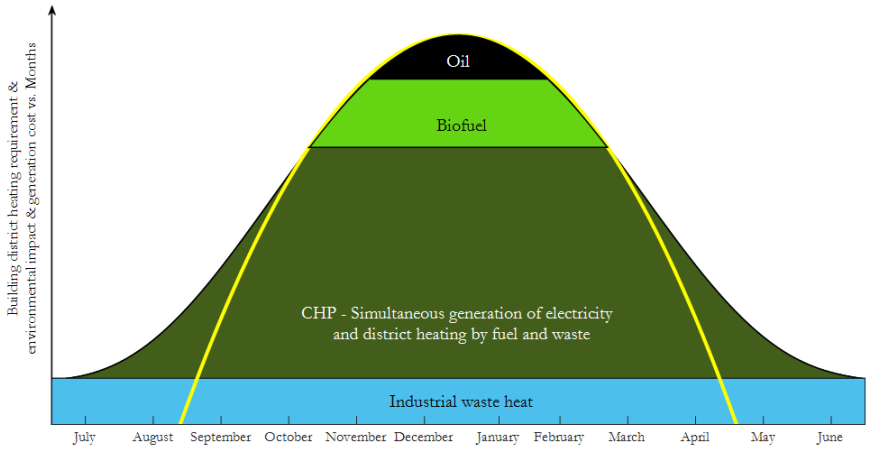

Figure 1.3: Annual buildings demand for district heating (DH) – The energy generation costs and environmental impacts (Levin and Karlsson, 2015)

Major thermal losses in buildings, especially in cold climate countries, are transmission heat losses, ventilation heat losses, and the thermal energy losses by discarded wastewater. Improvements in building materials, major retrofitting of existing buildings, and further insulation of buildings' envelopes in Sweden have resulted in decreased energy loss by infiltration and transmission. Swedish building regulations (BBR, 2018) were revised in 2018. Chapter 9 of the latest version provides the mandatory provisions and general recommendations on energy conservation. *"Buildings shall be designed in such a way that energy use is limited by low heat losses, low cooling demands, efficient use of heat and cooling and efficient use of electricity"*. Buildings shall meet the requirements for primary energy factors provided by BBR, and the suggested thermal transmittance (U-value) for all components of the building envelope shall be pursued.

The heating energy cost in district-heated areas in Sweden currently consists of both the total energy usage (kWh) and the thermal load (kW) during a year. Figure 1.4 illustrates the required heating energy and the energy cost of a multi-family building in the suburbs of Stockholm (Vattenfall, 2019). The heating demand of the building (2140 m2floor heated area) was 66 kWh/(m2floor heated area.year). The required thermal load cost can comprise 19–90% of the monthly expenditures, and annually it composes 37% of the total heating expenditures. Therefore, attention should also be given to buildings' heating load reduction in parallel to making efforts to reduce the buildings' heating energy demand.

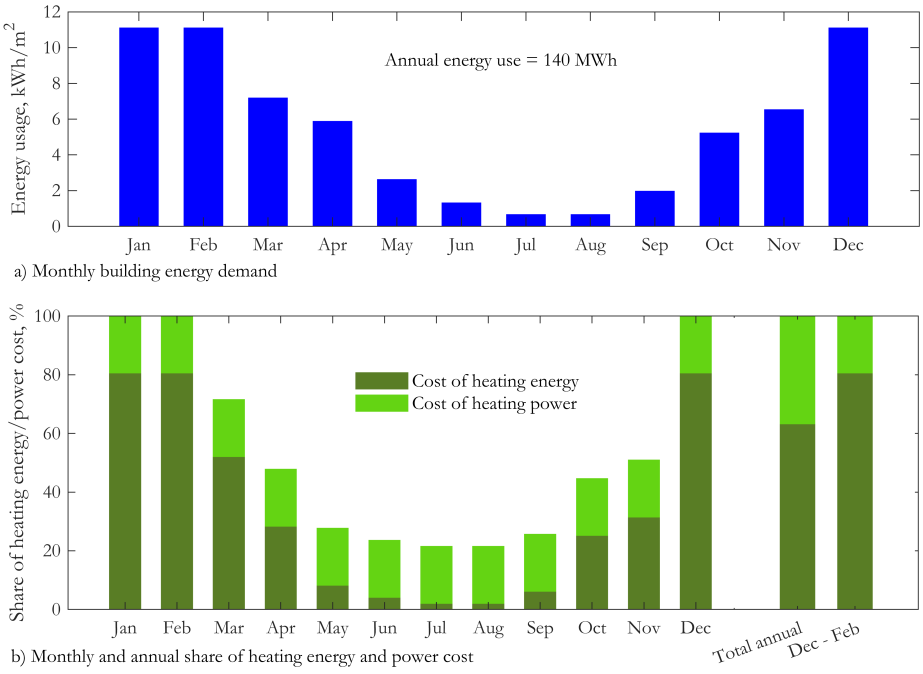

Figure 1.4: Monthly distribution of heating energy demand and the energy-power costs in a multi-family building

Moving from buildings constructed in the mid- and late 20th century to the current high thermal performance constructions, not only has the share of domestic hot water (DHW) heat demand not been equally improved, it has doubled (Meggers, 2011). Reducing the transmission thermal losses from a building by enhancing airtightness and insulation demands more effective ventilation systems to meet the building's indoor air quality (IAQ) requirements. Ventilation systems have to maintain the IAQ level and ensure the perceived thermal comfort standards. Although ventilation systems without heat recovery could provide the required amount of

fresh air, the ventilation heat losses in these systems are significant in cold regions. Therefore, the present study utilized a mechanical ventilation system with heat recovery (MVHR), with an annual energy recovery efficiency of up to 80%.

A significant drawback of MVHR systems is the formation of a layer of ice at the heat transferring surfaces of the heat recovery exchanger at low outdoor temperatures. Accumulation of frost in the heat exchanger reduces the heat transfer rate between the return air from the building and the fresh outdoor air. Other adverse effects are blockage of the return airflow, degradation of heat transfer surfaces, increased required fan power and compromised indoor air quality (Nasr et al., 2014, 2015; Song and Dang, 2018).

Various methods have been developed to remove the ice from the heat exchanger surface. Passive techniques such as changing surface morphology, anti-frost coating, and hydrophilic coating delay the initialization of frosting by reducing the amount of water on the cold surfaces. Active methods, such as low-frequency and ultrasonic vibrations, reverse cycle of hot gas, electric heater, and desiccants, are also effective in removing frost or delaying frost formation (Song and Dang, 2018). However, frost prevention is a more energy-efficient method for tackling frost problems (Nasr et al., 2015). The main frost preventative measures are return (room) air dehumidification and preheating the outdoor air before these two airflows are sucked in the MVHR. Electrical air preheaters are the most common method for increasing the outdoor air temperature prior to the heat exchanger. Of course, this method requires additional electricity consumption, which is a high-grade energy source.

Renewable heat sources can also be utilized as the preheating energy source instead of electricity. Relatively constant ground temperature compared to outdoor air temperature provides a fairly relatable thermal potential for heating and cooling purposes in buildings. In Sweden, geothermal energy has been utilized to preheat the incoming outdoor air to MVHR in recent studies between 2015 and 2018 (Kempe and Jonsson, 2015; Simanic, 2016; Sundin, 2018). The geothermal energy was extracted without using a heat pump in these studies.

The freezing onset in plate heat exchangers has been investigated in previous studies by Fisk et al. (1985, 1983). Depending on the humidity of the return air from building, frosting started at certain incoming outdoor air temperatures. In Paper 5, it was shown that in case of 30% relative humidity in return air, frost in a plate heat exchanger could be avoided by preheating the incoming air to the AHU to approximately -2.4°C (Nourozi et al., 2019). Table 1.1 lists the suggested preheating temperatures in a number of previous studies and a lack of consistency in the values.

Table 1.1: Focus of the appended papers

References	Frost threshold $^{\circ}C$	Indoor RH %	Return/room temperature $^{\circ}C$	Comments
Ploskić and Wang (2018)	-4.1 - -6.2	25 - 35	21.5 - 22	$\dot{m}_{supp}/\dot{m}_{ret} = 0.91$
Simanic (2016)	-5	Not reported	21 - 22	-
Fisk et al. (1985)	-4.8	30	20	Balanced ventilation
Pacak et al. (2019)	-4	26.1	20	$\eta_{HX} = 70\%$
Huber (2019)	-2.7	Not reported	21	$\eta_{HX} = 80\%$
Nourozi et al. (2019)	-2.2	30	19	$\dot{m}_{supp}/\dot{m}_{ret} = 0.91$
Kragh et al. (2007)	-6	55 - 60	22.5	Switches between HXs
Anisimov et al. (2015)	-1.3	30	20	$\eta_{HX} = 60\%$
Anisimov et al. (2015)	-2	30	24	$\eta_{HX} = 60\%$

An alternative approach to avoid frost formation in heat exchanger is to generate different airflow rates in supply and return ducts by fans. The heat exchanger plate temperature is exposed to higher return airflow rates with a higher temperature than the supply air increases, and helps postpone condensation and frost formation or eliminating the accumulated frost. These two methods require precise knowledge of frosting and condensation start heat exchangers. Defining the frosting onset based on the relative humidity of the return air, outdoor air temperature, ventilation flow imbalance rate, and heat exchanger design characteristics provides the possibility of utilizing preventative measures to avoid frost formation and growth in the air pathways.

1.2 Research objective

The main objective of this PhD work has been to propose, investigate, and evaluate possible approaches to reduce the peak thermal capacity demand of residential buildings in the Swedish climate. To accomplish this goal, the thermal potential of two primary sources of heat losses from buildings were studied in the first step: wastewater and ventilation air.

Secondly, I investigated the effect of utilizing an air preheater installed before the heat exchanger at the air handling unit on the energy-saving potential and decreasing the defrosting need. The aim was to target the peak heat loads during the coldest days in winter when defrosting the heat exchangers essentially increases the

peak heating load even more. The goal was to use the heat from the outgoing wastewater from the building to preheat the incoming outdoor airflow to MVHR and reduce the defrosting need during the coldest days. This also included a detailed heat transfer modeling of a ventilation air-to-air heat exchanger to inspect the condensation onset during various working conditions.

Lastly, I studied the performance of a novel window type called the energy-active window (EAW) in reducing buildings' peak thermal capacity demand.

1.3 Hypothesis

"Buildings' thermal load demand will be cut by preventing frost formation in the ventilation heat exchanger."

1.4 Overview of publications

This thesis is a summary of seven appended publications. The focus of each of the publications concerning the research items is presented in Table 1.2.

Table 1.2: Focus of the appended papers

Publication / **Item**	Paper 1	Paper 2	Paper 3	Paper 4	Paper 5	Paper 6	Paper 7
Peak thermal shaving	X	X	X	X			
HX freezing	X	X	X		X		
Control		X	X		X	X	
Waste heat recovery	X	X		X		X	
Geothermal utilization		X		X			
LCC							X

Figure 1.5 illustrates the connection between Papers 1-6 and how they contributed to the main objective of this PhD work, shaving the building peak thermal demand.

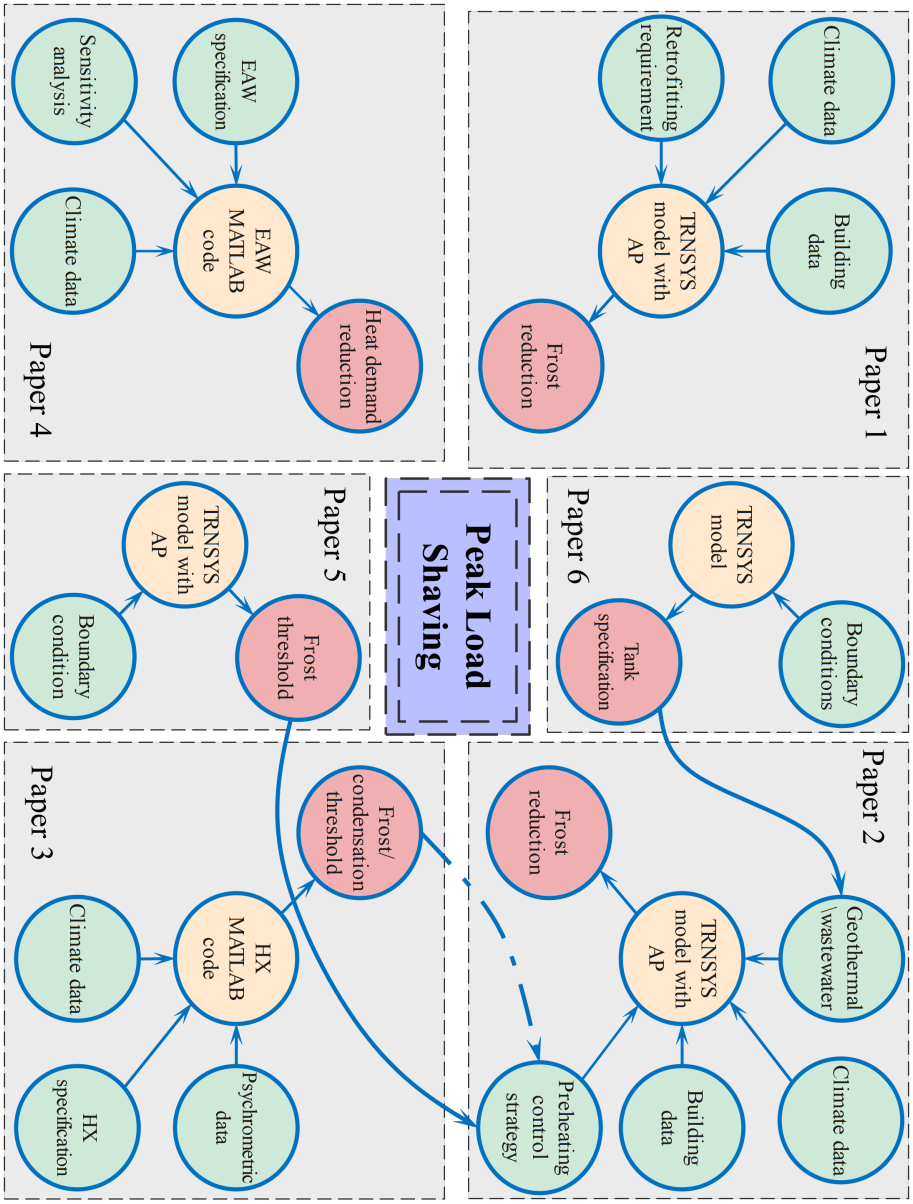

Figure 1.5: Overview of research process, showing how publications contribute to the research question

Chapter 2

Methodology and Tools

In this PhD work, various tools and methodologies were adopted to evaluate either components' or a system's thermal performance. Energy simulation tools such as TRNSYS have been used to investigate the energy demand of the target buildings. Life cycle cost (LCC) analysis has been used to examine the cost-saving potential of the studied heat recovery systems compared to their potential in energy savings. Analytical methods and semi-numerical simulations have been utilized by coding detailed heat transfer mechanisms in Matlab to obtain temperature distribution in the EAW and detect the condensation point in a heat exchanger.

2.1 Energy systems analysis

Papers 1 and 2 present a simulated building equipped with mechanical ventilation with heat recovery. The ventilation heat exchanger could be frozen and clogged by being exposed to cold outdoor air. As a common sustainable approach, air preheating has been used to lift the outdoor temperature above the frosting threshold. Thermal energy in residential wastewater is an available source of energy that was recovered and used in the air preheater before the wastewater was discarded. Figure 2.1 illustrates the investigated wastewater air preheaters.

Two outdoor air preheating systems that benefit the thermal potential of residential wastewater were suggested, and their performance was evaluated by dynamic simulations. The discarded wastewater was stored in a black water cleaner before being accumulated in a thermal storage tank. Despite large-scale wastewater separators being more commonly used in wastewater treatment plants, smaller devices are currently developed and are available on the market Huber; SHARC. The performance of the black water cleaner was not within the scope of this research work; however, it was assumed that the outgoing greywater was sufficiently purified to be pumped to a water-to-air heat exchanger. This greywater (wastewater is often used in this text and the appended papers) was stored in two storage tanks, a temperature stratified and an unstratified tank; see Figure 2.1. A pump circulated the wastewater to a water-to-air heat exchanger where the outdoor air could be preheated before entering the MVHR. The following subsections provide information about the methodologies used to evaluate the studied air preheating systems. More details are available in Paper 2.

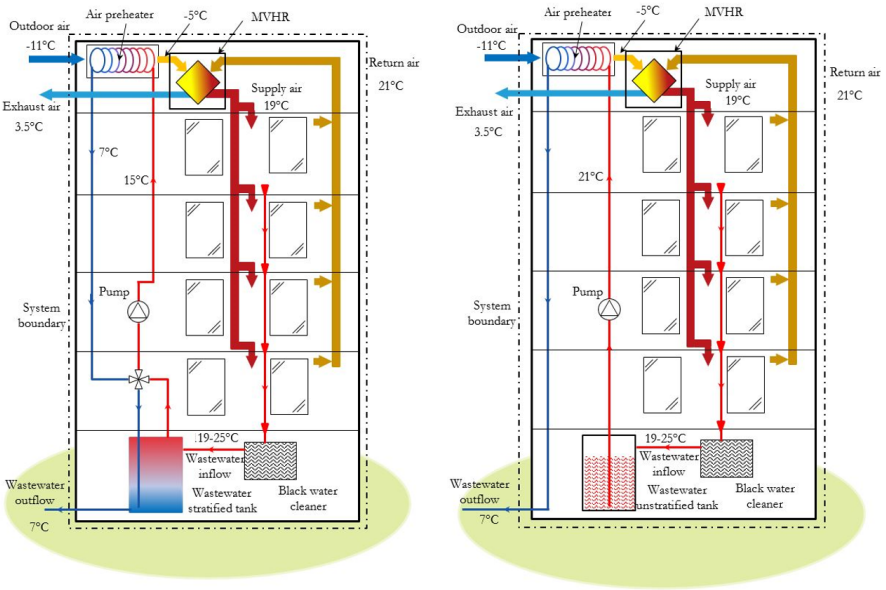

Figure 2.1: Schematic flow charts of the studied air preheating systems using wastewater from the stratified tank (left) and the unstratified tank (right)

2.1.1 Simulation tools

The principal method utilized in this research work was dynamic simulations using the commercial software TRaNsient SYstem Simulation Program, TRNSYS 17. TRNSYS is a transient simulation software capable of simulating several dynamic systems, such as thermal and electrical energy systems and traffic flow. The extensive libraries in TRNSYS enable users to select from among the available components while there is the possibility of modifying or creating new ones for specific purposes.

The processing engine in TRNSYS (kernel) iteratively solves the systems made by several components from the libraries. TRNSYS original solver, Solver 0 or successive substitution starts from a component and obtains the outputs by solving its equations using the initial inputs. This continues to the other components and the output from the last component can be the first component's input. A tolerance between the initial input and the last obtained output will define the convergence for the first time-step. After convergence is reached in every time-step, the same loop will be repeated for the next one and this will continue for the entire simulation period.

Several building models from different climatic zones in Sweden have been utilized

to evaluate the performance of the suggested systems. Since the focus of the study was on the ventilation system and the proposed air preheating systems, a single zone model (Type660) represented the considered buildings. However, all models were validated by the measured data provided in reference studies.

The built-in climatic files in TRNSYS for Europe were used in all simulations. These files were generated using Meteonorm under license from Meteotest and verified by Weather in Stockholm. Meteonorm is capable of generating a typical representative year of any place on earth by choosing up to 30 or more different climatic parameters. Hourly climatic data, as well as the user input data, contributed to performing more realistic energy simulations. The hourly information of the outgoing wastewater temperature and flow rate and defining the heat recovery efficiency of MVHR as a function of inlet air temperature were the main user input files to TRNSYS.

2.1.2 Investigated systems

This subsection briefly summarizes the heat recovery systems from the building's ventilated air and residential wastewater. Two multi-family buildings were modeled in TRNSYS. Both buildings were equipped with mechanical ventilation with heat recovery systems. The building in Stockholm utilized a rotary heat exchanger in the MVHR, and the building in Örebro was equipped with a plate heat exchanger. The difference in the heat exchanger type resulted in various defrosting requirements and frosting thresholds. Various previous measurement studies have shown that the defrosting heat load is approximately 6.2 $W/m^2_{floorarea}$ (Kempe and Jonsson, 2015; Orpana, 2016; Simanic, 2016; Sundin, 2018). A recent study by Ploskić and Wang (2018) has revealed that the thermal potential of residential wastewater was sufficient to avoid frosting in MVHR systems; see Figure 2.2.

Figure 2.3 shows the case of a multi-family building located in the southern Swedish city of Växjö (Le Truong et al., 2014) and depicts the building's heating power demand with and without a mechanical ventilation heat recovery system during a year. By installing an MVHR system, the required heating power was decreased by 5–20 kW during the year. The green line shows the reduction in load demand by using the MVHR system (thermal power saving). However, this was not achieved since frosting occurred during the winter period. The outdoor temperature in Växjö is below -5°C for about 30 days a year. This temperature is the frosting threshold of a plate heat exchanger. Therefore, a plate heat exchanger requires 6.2 $W/m^2_{floorarea}$ heating power to defrost; see Figure 2.3 (dashed purple line). Despite the significant reduction of building heat load by installing an MVHR system, the temperature (heat recovery) effectivity of the heat exchanger can be reduced from 80–90% to 30–40% during defrosting mode due to frosting (Simanic, 2016).

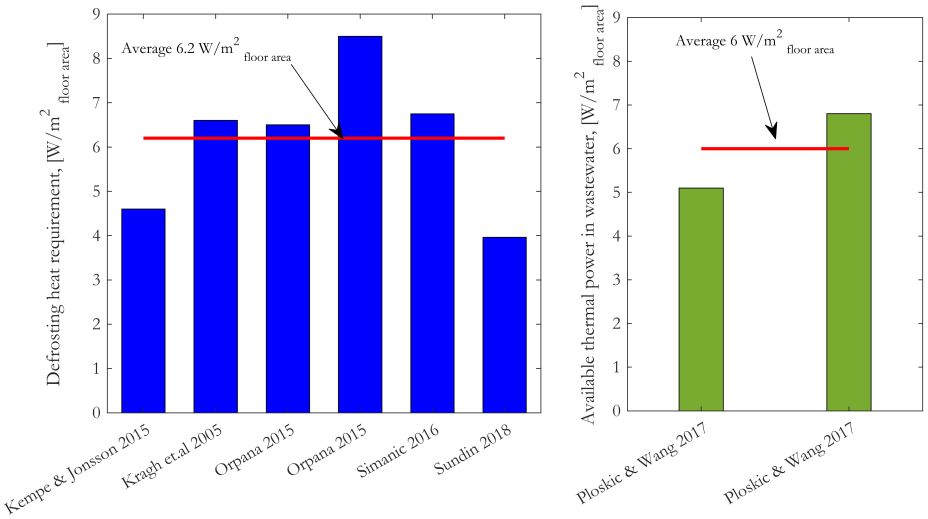

Figure 2.2: The average required heating power for defrosting and the available wastewater thermal potential

2.1.3 Model validation

The main components in each simulation model presented in the appended papers were validated by measured data reported by others. The building models that were continuously in response to the MVHR system were the main validation cases for energy simulations. The building cases' annual and monthly heating energy demand was validated against the measured data by the presented references. The detailed information regarding the building model verification is provided in Paper 1. The performance of the outdoor air preheating system was validated with measurement data from similar preheating systems. In Paper 1, the simulated air temperature increase range versus the outdoor air temperature was plotted and compared with the corresponding measurements (Nourozi et al., 2019). Since each measurement study had specific settings, the increase in air temperature was weighted by the recovered heat power from circulated water and the air mass flow rate for each case. Therefore, the ratio of the preheated air temperature to the unit specific enthalpy is plotted against the outdoor air temperature in Figure 2.4.

In the outdoor temperature span, of between -20°C and +5°C, the deviation between the simulated and the measured values was less than 1°C/(kJ/kg). All considered systems followed the same increase trend. The simulated air preheater in Paper 2 was validated against measurements for two short periods with moderate and cold outdoor temperatures in in Örebro in November and January, respectively (Nourozi et al., 2019). The average percentage differences between simulated and measured temperatures were 6.6% and 12.0% in November and January, respec-

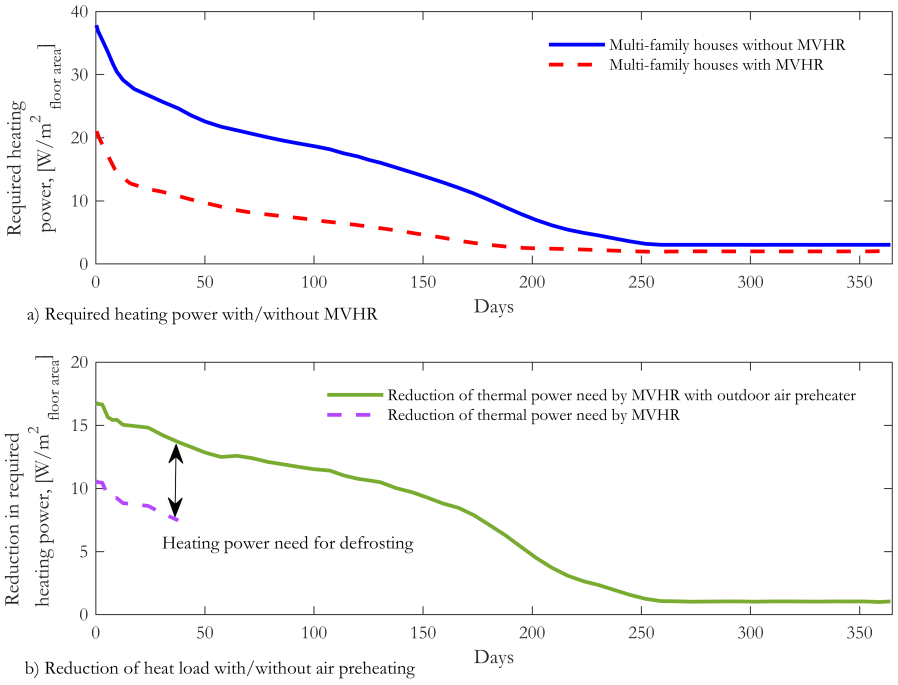

Figure 2.3: Energy saving potential in multi-family buildings by MVHR (Le Truong et al., 2014)

tively.

The Standard Error of Estimate (SEE) was used to rate the deviation between the simulated and the measured values for January. The SEE value for the measured and simulated cases was 1.7°C, and the simulated temperature was close to the measured temperature line except for a few hours when the circulation pump was off. As can be seen from Figure 2.5, the simulated values were within the range of $\pm 1.5 \times$SEE ($= \pm 2.5$°C) for almost the entire studied period. More details about validation for this part can be found in Paper 2.

2.2 Life cycle cost (LCC) analysis

Life cycle cost analysis was used to assess the cost-effectiveness of the investigated outdoor air preheating systems. The assessment of the analyzed heat recovery systems underwent life cycle cost analyses further to their energy and power-saving potential. The Directive, 2010/31/EU of the European Parliament and of the Council on the energy performance of buildings, has established a framework for calculating cost-optimal minimum energy performance requirements for buildings

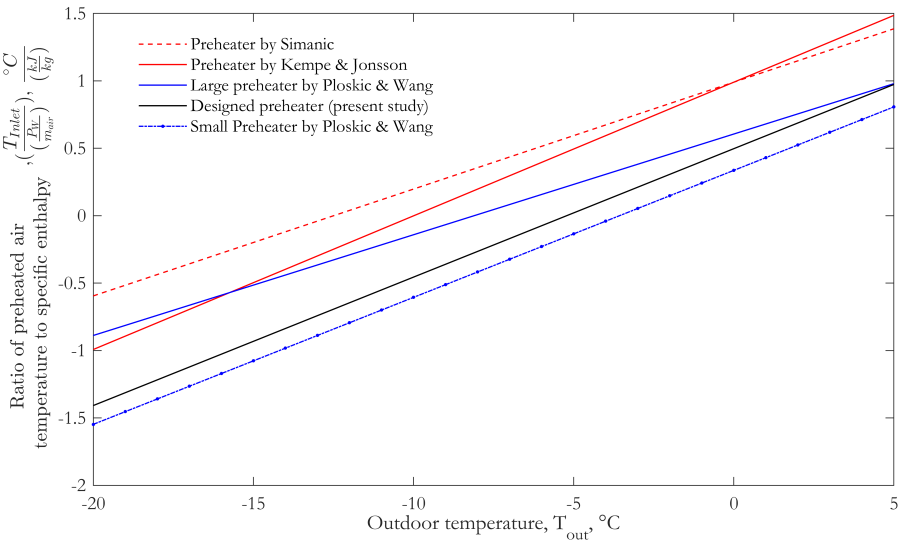

Figure 2.4: Weighted preheated air temperature to MVHR by specific enthalpy (Nourozi et al., 2019)

((EU) No 244/2012, 2012). This directive provides the general principles of cost calculation and categories of costs, which comprise the basis of the LCC analysis in this work.

The net present value (NPV) method was used to evaluate the cost-effectiveness of the suggested air preheating systems. NPV is used for products and processes in which most expenditures are required after the initial investment. The calculation considers the value of the money at the time, inflation, initial investment costs, and cash flow. More details can be found in a thesis by Härer (2019).

The cash flow in each period can break down into maintenance costs, energy costs, repair and replacement costs, and recycling costs. The initial costs include manufacturing price, installation costs, sales tax, and retail markups (Härer, 2019). Comparing the cumulative costs of the studied systems with a base system (the building equipped with MVHR without an air preheating system) can indicate the discounted payback period. The payback time of each system is the duration before reaching a break-even point where the expended initial investment is regained due to savings by using more energy-efficient equipment.

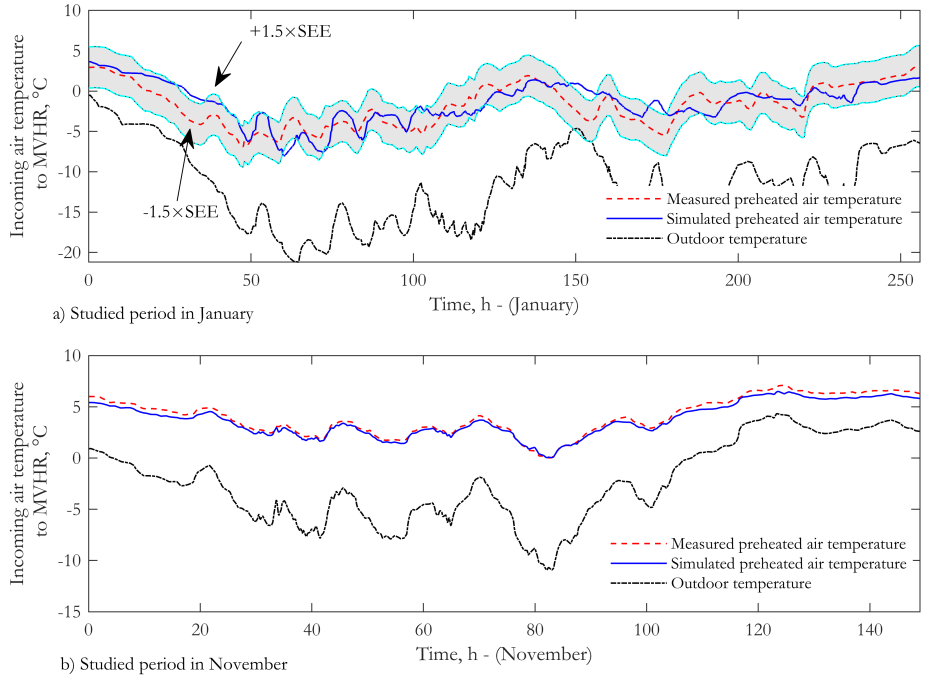

Figure 2.5: Preheated air temperature, TRNSYS simulation versus field measurements (Nourozi et al., 2019)

2.3 Heat transfer analysis

Papers 3 and 4 present detailed heat transfer modeling of a ventilation heat exchanger and an energy active window using a semi-numerical methodology in Matlab. Paper 3 defines the condensation and frost thresholds of a ventilation counterflow heat exchanger under various working conditions. Paper 4 provides a detailed thermal transmittance analysis of an EAW and design guidelines for this type of window under extreme winter climate conditions.

2.3.1 Condensation and frosting in ventilation heat exchanger

Paper 3 presents the detailed heat transfer modeling in a ventilation heat exchanger. In order to effectively adopt a preventative measure for tackling the frosting problem in ventilation heat exchangers used in Papers 1 and 2, precise condensation and frosting onsets should be known. Condensation depends on the cold stream temperature and the relative humidity of the warm stream. These two parameters in the ventilation case are the outdoor air temperature and relative humidity of the return air from buildings. Figure 2.6 illustrates the fluctuation of indoor rela-

tive humidity with outdoor temperature for a Swedish residential building during the winter season when the risk for condensation is high. Indoor relative humidity ranges between 10-40% and the outdoor temperatures range from -20° to 0°C.

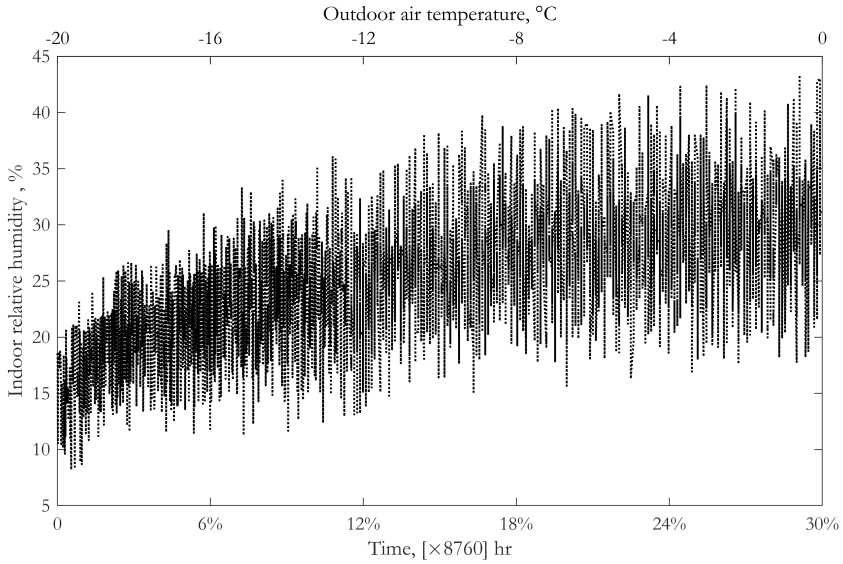

Figure 2.6: Variation of outdoor temperature and indoor relative humidity in a Swedish residential building during winter season

Simulation model and utilized tool

This section defines the heat transfer rate and temperature distribution along the heat exchanger length using semi-numerical simulations in Matlab. The simplified geometry of the heat exchanger shown in Figure 2.7 was used for this purpose. The consecutive parallel plates and the hot and cold airstreams from indoor and outdoor represent a repetitive symmetry across the heat exchanger width (j-direction). It was also assumed that every adjacent supply and return air stream and the plate that keeps them apart had the same temperature distribution. Thus, analyzing two adjacent air streams and the separating plate represented the entire heat exchanger.

The temperature distribution in the air channels defines the plate temperature, which affects condensation. A two-dimensional upwind scheme was applied to the steady-flow energy equation and Newton's law of cooling for the discretized domain to calculate the air and plate temperatures at each cell. Equations 2.1, 2.2, and 2.3 were utilized to calculate the air temperature at the supply and return airstreams and the separating plate temperature.

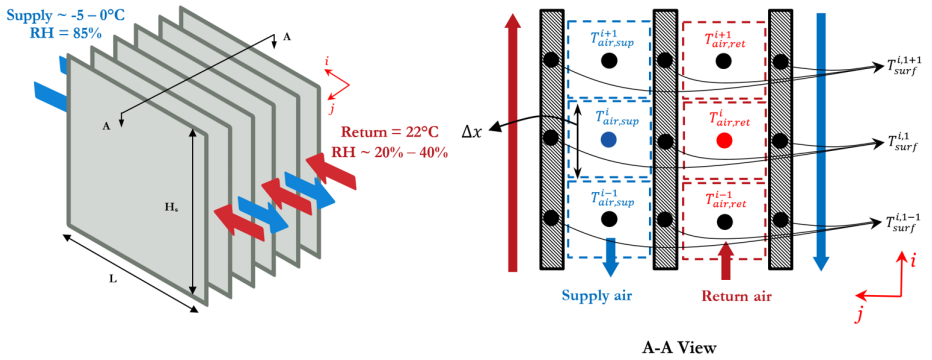

Figure 2.7: Simplified geometry of the studied counter-flow HX and how it is discretized

$$T^i_{air,ret} = \frac{\dot{m}_{ret} c_{p,ret} T^{i-1}_{air,ret} + 2H_s \Delta x h^i_{ret} T^i_p}{\dot{m}_{ret} c_{p,ret} + 2H_s \Delta x h^i_{ret}} \tag{2.1}$$

$$T^i_{air,sup} = \frac{\dot{m}_{sup} c_{p,sup} T^{i+1}_{air,sup} + 2H_s \Delta x h^i_{sup} T^i_p}{\dot{m}_{sup} c_{p,sup} + 2H_s \Delta x h^i_{sup}} \tag{2.2}$$

$$T^i_p = \frac{k_p \frac{tH_s}{\Delta x}(T^{i-1}_p + T^{i+1}_p) + H_s \Delta x (h^i_{ret} T^i_{air,ret} + h^i_{sup} T^i_{air,sup})}{2k_p \frac{tH_s}{\Delta x} + H_s \Delta x (h^i_{ret} + h^i_{sup})} \tag{2.3}$$

The convective heat transfer coefficients on the plate for both sides were defined from the adjacent air stream cells. Air in both sides was driven by fans, and considering the uniform distribution of air in all air slots, the resulting Reynolds number was between 600 and 800. The critical Reynolds number for parallel plates in heat exchangers suggested by Hesselgreaves et al. (2016) is below 2200. The Richardson number obtained by simulations was approximately 0.1. Previous references have suggested Ri = 0.25 for the limit of forced convection (Papanicolaou and Jaluria, 1991; Raji and Hasnaoui, 1998; Singh and Sharif, 2003). Therefore, the heat transfer mechanism in both slots was laminar forced convection and the coefficient was calculated by Equation 2.4 suggested by Edwards et al. (Bergman et al., 2017).

$$Nu = \frac{hD_h}{k_{air}} = 7.54 + \frac{0.03(D_h/L)RePr}{1 + 0.016[(D_h/L)RePr]^{2/3}} \tag{2.4}$$

Equation 2.4 is valid for part of the domain where the air is dry. The air properties were updated for each discretized cell during simulations using the built-in psychrometric relations provided in Paper 4 for humid air. In other words, when the humid air temperature exposed to cold plate falls below the dew point temperature, the water content of air condensates. In this condition, the conductive heat transfer between plate and fluid changes, since a layer of condensate is in contact with the plate. Wang and Zhao (1993) provided an experimental Nusselt correlation (Equation 2.5) to predict the heat transfer coefficient for the wet part of the heat exchanger.

$$Nu = 0.0015(Re_l/H)^{0.983} Pr_l^{0.33} (\rho_l/\rho_v)^{0.248} \tag{2.5}$$

where

$$Re_l = G(1 - \dot{x}_{out}) D_l/\mu_l \tag{2.6}$$

$$H = \frac{c_{p,l}(T_{sat} - T_p)}{\Delta h_v + 0.68 c_{p,l}(T_{sat} - T_p)} \tag{2.7}$$

$$G = \frac{\dot{m}}{A_{crosssection}} = \frac{\dot{m}}{H_s d_s} \left[{}^{kg}/_{m^2 s}\right] \tag{2.8}$$

Equations 2.6 - 2.8 define the Reynolds number of the fluid in the wet section Re_l, the dimensionless parameter for providing the influence of subcooling of the condensate H, and the mass velocity G.

Model validation

The validity of the developed heat exchanger model is verified by measurement data for the supply air temperature to the building from a Swedish ventilation heat exchanger manufacturer. Further validation of the Matlab code in predicting the frosting threshold was conducted by measurement data previously reported by Fisk et al. (1985).

Figure 2.8 draws a comparison between the simulated supplied air temperature and the corresponding measured data at a constant outdoor air temperature of

0°C for indoor relative humidities ranging between 10% and 50%. The maximum relative deviation between our simulation results and the data provided by the manufacturer is 8.2%.

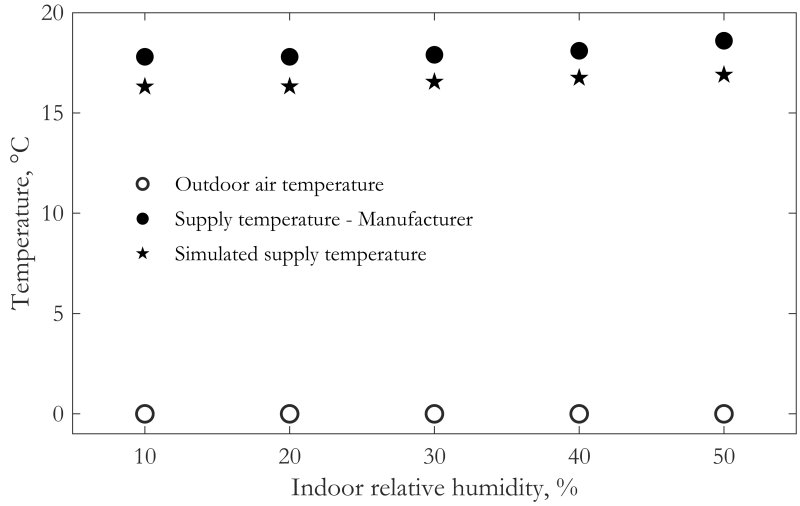

Figure 2.8: Simulated vs. measured supplied air temperature to building

The simulated frost threshold in the heat exchanger under different working conditions was also compared by a similar experimental study carried out by Fisk et al. Fisk et al. (1985). Figure 2.9 illustrates the simulated and measured frost thresholds during various working conditions of a ventilation heat exchanger. The heat exchanger was exposed to indoor relative humidity between 25% and 58%. These sets of temperatures similarly divided the figure into two sections: "freezing" and "no freezing". For each indoor relative humidity value, temperatures above the division line define a working condition without freezing, and for lower temperatures, freezing occurred in the heat exchanger. The maximum deviation between the simulated and measured frost thresholds was 11%.

2.3.2 Energy-active window – A complement to heating systems

Paper 4 concerns the heat transfer modeling across the EAW cross-section. The interior surface temperature of a window impacts the indoor operative temperature, perceived indoor thermal comfort, and rate of heat loss from the window. Therefore, a detailed heat transfer study on the interior and exterior window surfaces was carried out in Paper 4, and the methodology is summarized in this section.

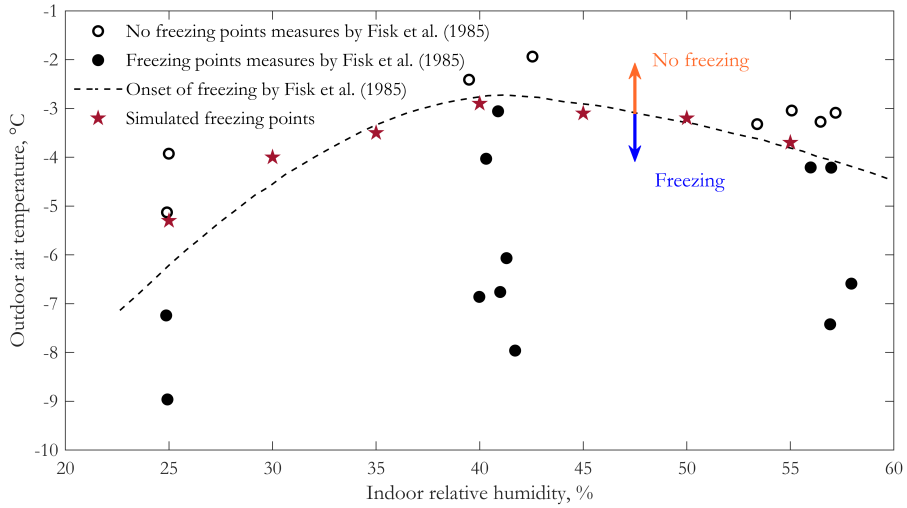

Figure 2.9: Simulated frost thershold vs. measurement data in a ventilation heat exchanger

Simulation model and utilized tool

Figure 2.10 shows the studied energy active window. The configuration was similar to a double-glazing window, but there was a closed air loop between the glazings. The middle glazing assembly, excluding the closed air loop, was a super-insulated double-pane window filled with argon. A fan mounted on a heat exchanger, which served as one component, was installed underneath the window to circulate warm air in the slots.

A two-dimensional upwind differencing scheme was applied to the discretized model, as shown in Figure 2.11, to approximate the vertical and transverse temperature distribution between the window panes. Equations 2.9 - 2.11 were used in the developed Matlab code to calculate air and panes' temperature along the window height.

$$T_{air}^{i} = \frac{\dot{m} c_{p,air} T_{air}^{i-1} + b\Delta x \sum_j h_{conv}^{i,j} T_{surf}^{i,j}}{\dot{m} c_{p,air} + b\Delta x \sum_j h_{conv}^{i,j}} \tag{2.9}$$

$$T_{surf}^{i,j} = \frac{k\frac{bt}{\Delta x}(T_{surf}^{i-1,j} + T_{surf}^{i+1,j}) + b\Delta x(h_{rad}^{i,j} T_{surf}^{i,j} + h_{conv}^{i,j} T_{air}^{i,j} + h_{in|out} T_{in|out})}{k\frac{bt}{\Delta x} + b\Delta x(h_{rad}^{i,j} + h_{conv}^{i,j} + h_{in|out})} \tag{2.10}$$

$$T_{surf}^{i,j} = \frac{k\frac{bt}{\Delta x}\left(T_{surf}^{i-1,j} + T_{surf}^{i+1,j}\right)}{k\frac{bt}{\Delta x} + b\Delta x\left(h_{rad}^{i,j-1} + h_{conv}^{i,j} + h_{rad}^{i,j+1} + h_{argon}\right)} + \frac{b\Delta x\left(h_{rad}^{i,j-1}T_{surf}^{i,j-1} + h_{conv}^{i,j}T_{air}^{i,j} + h_{rad}^{i,j+1}T_{surf}^{i,j+1} + h_{argon}T_{argon}\right)}{k\frac{bt}{\Delta x} + b\Delta x\left(h_{rad}^{i,j-1} + h_{conv}^{i,j} + h_{rad}^{i,j+1} + h_{argon}\right)} \tag{2.11}$$

where $\dot{m}$ is the air mass flow rate, $h_{conv}^{i,j}$ is the convective heat transfer coefficient in previous control volume, $h_{rad}^{i,j}$ is the radiative heat transfer coefficient with the window panes across the window, Δx is the grid size along the window height, b is the window width, and T_{surf}^{i} is the temperature at window panes across the window cross-section. $T_{in|out}$ and $h_{in|out}$ are the indoor/outdoor temperatures and the heat transfer coefficients at the interior/exterior glazing, respectively.

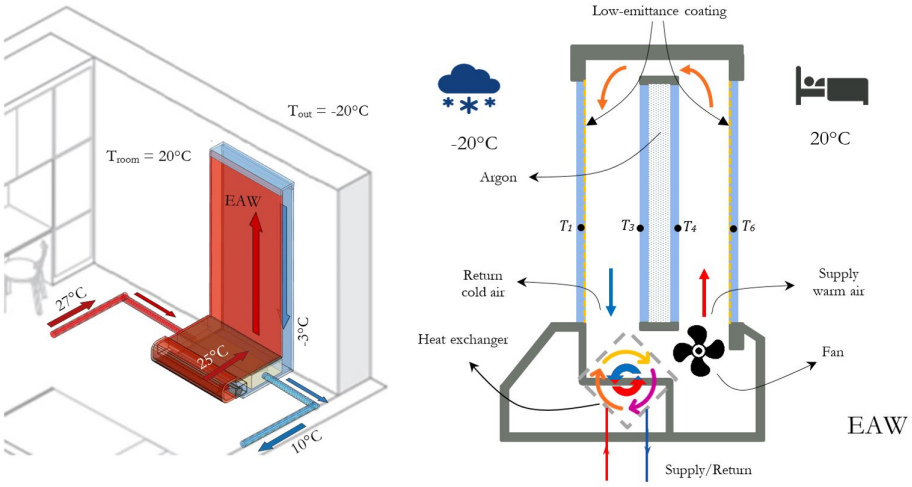

Figure 2.10: Schematic of EAW configuration and installation in the building (Nourozi et al., 2020)

Radiative and convective heat transfer are the dominant mechanisms in the window configuration. The thermal resistances in the window cross-section are in series. Therefore, the largest value considerably affects the total thermal transmittance across the window. In this investigation, a commonly used value of peak load calculation for the exterior heat transfer coefficient, h_{out}, in winter was used. The convective heat transfer coefficient on the interior window surface was approximated using Equation 2.12, an empirical correlation for calculating the average Nusselt

number for natural convection over a vertical surface suggested by Churchill and Chu (1975).

$$Nu_{in} = \left[0.825 + \frac{0.387 Ra_L^{1/6}}{\left[1 + \left({}^{0.492}/_{Pr_{in}}\right)^{9/16}\right]^{8/27}}\right]^2 \tag{2.12}$$

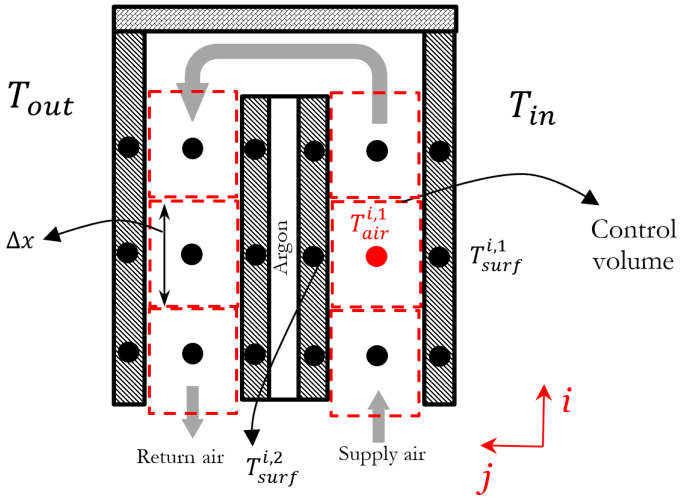

Figure 2.11: Discretization of simplified EAW geometry

The convective heat transfer coefficient in the slots depended on the type of convective regime. The Richardson number $\left(Ri = {}^{Gr}/_{Re^2}\right)$ value defined the correct correlations for natural, mixed, and forced convection in the slots. Suggested values of $Ri = 0.25$ and $Ri = 4$ are the limits for forced, mixed, and natural convection. Richardson numbers above 4 imply that inertia forces are negligible and natural convection is dominant. In this case, natural convection in the slots was the main convective regime, and the Nusselt correlation (Equation 2.13) suggested by Bar-Cohen and Rohsenow (1984) was used for vertical isothermal parallel plates with asymmetric temperatures.

$$Nu = \left[\frac{144}{(Ra_{d_s})^2} + \frac{2.873}{(Ra_{d_s})^{1/2}}\right]^{-1/2} \tag{2.13}$$

In the case of a Richardson number below 0.25, forced convection is the primary heat transfer mechanism, and buoyancy forces are neglected in this regime. A modified version of Equation 2.4 for laminar forced convection between parallel plates with asymmetrical temperatures was used. The modification to Equation 2.4 is based on the plates' temperatures symmetry by Shah and London (2014), presented in Equation 2.14.

$$\begin{Bmatrix} If & T_{W1} \neq T_{W2} & Nu_1 = Nu_2 = 4 \\ If & T_{W1} = T_{W2} & Nu_T = 7.54070087 \end{Bmatrix} \tag{2.14}$$

Mixed convective heat transfer is dominant at a middle range of Richardson number between 0.25 and 4, and the corresponding Nusselt number can be calculated by Equation 2.15 (Bergman et al., 2017; Cengel and Ghajar, 2014).

$$Nu_{mixed} = \left(Nu_{forced}^3 + Nu_{natural}^3 \right)^{1/3} \tag{2.15}$$

Model validation

The developed Matlab code for simulating the heat transfer in windows cross-section was validated in two stages: a triple-glazed window studied experimentally by Larsson et al. (1999) and an EAW prototype investigated by Bergman (2009).

Figure 2.12 draws a comparison between the simulated and measured temperatures on the glass surfaces of a triple-glazed window for two outdoor and indoor temperatures. Good agreement was achieved between both sets of data.

Bergman (2009) previously investigated the performance of an EAW prototype and reported the return air and inner glazing temperatures in a demonstration building. The simulation setup followed the instructions provided for the measurements, as presented in more detail in Paper 4. The comparison of the obtained simulated and measured data for various airflow rates is shown in Figure 2.13.

The airflow rate injected to EAW varied between 4.5-11 L/s. The temperature of the inner glazing was reported at four points on the pane to determine the transverse and vertical temperature gradients. As can be seen in Figure 2.13a, with the increased airflow rate, the measured and the simulated return air temperatures diverged. The best agreement was reported at an airflow rate of 4.5 L/s, and

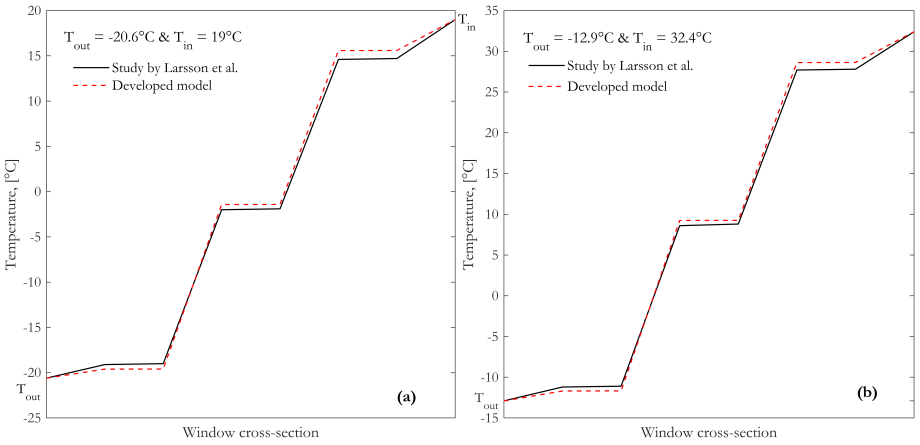

Figure 2.12: Comparison of simulated and measured temperature across window width

the maximum deviation was 2°C (12%) at an airflow rate of 11 L/s. According to Figure 2.13b, the maximum temperature difference between the simulated and measured inner glazing temperatures was approximately 0.7 °C (4%) at a flow rate of 11 L/s.

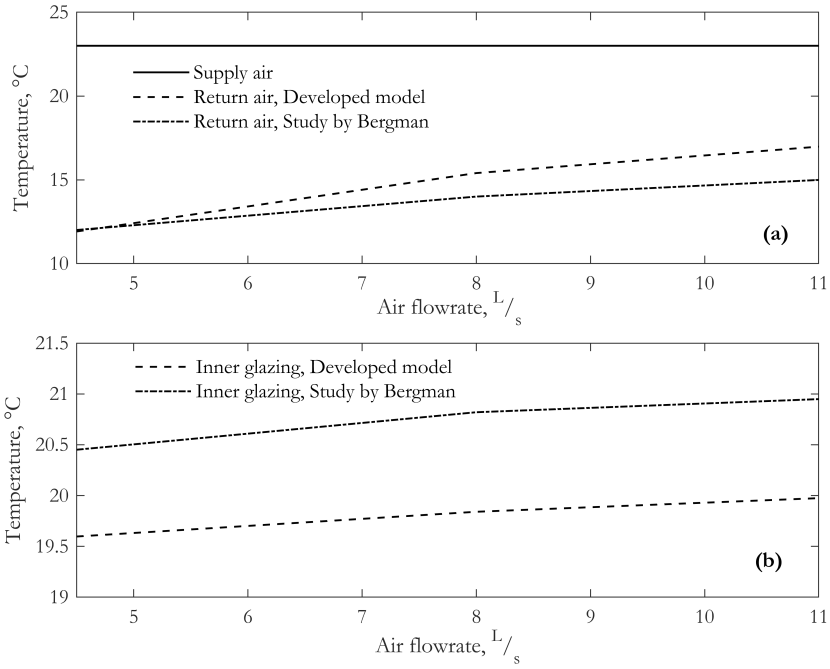

Figure 2.13: EAW inner glazing temperature, simulation vs. measurement

Chapter 3

Results and Discussion

This section presents a brief review of the most important results of the conducted research. More detailed discussions and results can be found in the appended papers.

Papers 1 and 2 mainly presented the results regarding the performance evaluation of the suggested heat recovery system. Papers 5 and 6 showed the results of the potential of the wastewater storage and the reduction of the defrosting need in the heat recovery exchanger, respectively. Paper 7 presented an evaluation of the studied energy systems in terms of cost-effectiveness

3.1 Energy systems analysis

Figure 3.1 illustrates the MVHR system with an air preheater, with the associated notations.

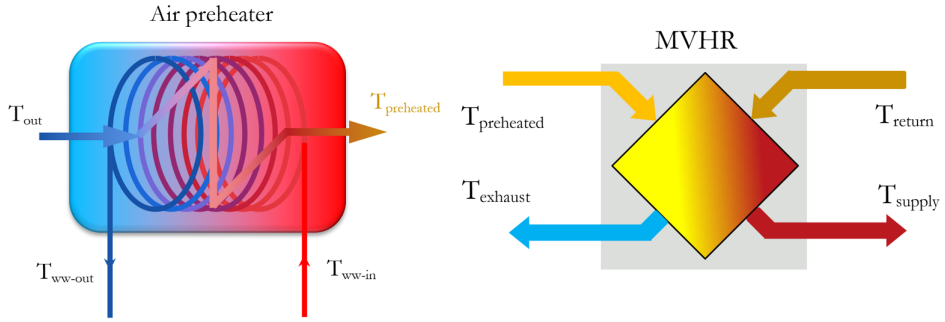

Figure 3.1: The air preheater and MVHR system

Papers 1 and 2 mainly focused on evaluating the potentials of an outdoor air preheating system using wastewater heat and geothermal energy to preheat the incoming air to MVHR. TRNSYS simulation results of a multi-family building in Stockholm proved that the wastewater air preheater could increase the inlet temperature to above the frost threshold for most of the period; see Figure 3.1. In Paper 1, it was shown that the initial defrosting period (without air preheating) for a plate heat exchanger was reduced by 50%. In the case of an MVHR equipped

with a rotary heat exchanger, frosting need was eliminated for the entire heating season.

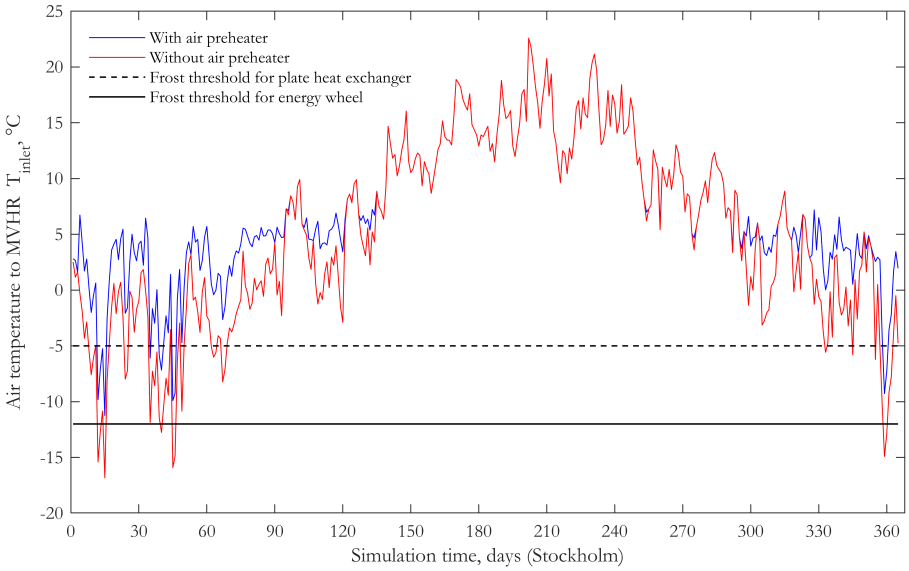

Figure 3.2: Chance of frost formation in MVHR served with and without air preheating (Nourozi et al., 2019)

However, the preheated air temperature shown in Figure 3.2 was not controlled to just above the frost threshold. Identifying the frost threshold was vital in order to optimally use the thermal potential of the stored wastewater when required and maintain the efficiency of MVHR at the highest allowable value. In Paper 5, the frosting threshold for an MVHR system equipped with a plate heat exchanger was investigated. Return room air with an average relative humidity of 30% was studied to find the heat exchanger surface temperature and the frosting threshold.

Figure 3.3 illustrates the incoming air temperature to MVHR below which frosting starts at the surface of the heat exchanger. The studied period was bounded to part of the heating season when there was a chance of frosting in the heat exchanger, which was approximately five months in Örebro.

Figure 3.3 shows that frosting in the heat exchanger in MVHR started when the outdoor temperature was below -2.2°C. The frosting threshold can vary with the return air relative humidity; therefore, the air preheater operated for inlet temperatures below -3°C.

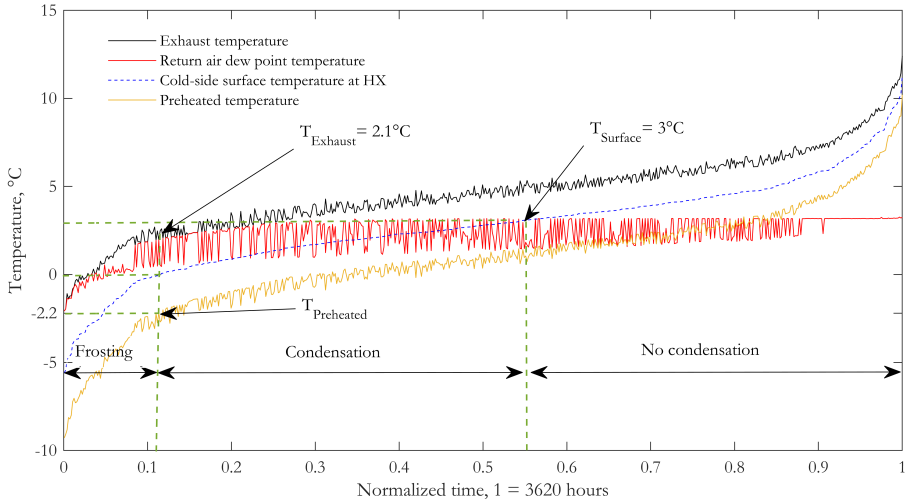

Figure 3.3: Frosting threshold in a plate heat exchanger by controlling the preheated air temperature (Nourozi et al., 2019)

In Paper 2, the effects of utilizing a preheated air temperature control were investigated in more detail. Figure 3.4 depicts the frosting duration for air preheating systems with and without a temperature control system. The simulated period for this case was also bounded to the part of the heating season when frosting was expected, which was four months. The defrosting period for both was reduced to approximately less than 10% of the evaluation time, but the preheated air temperatures were different. Therefore, controlling the preheated outdoor air temperature did not affect the defrosting period. However, preheated outdoor air temperatures significantly above the frost threshold negatively influenced the heat recovery efficiency of the MVHR system.

Papers 1 and 2 studied the effect of utilizing a temperature control system on the heat recovery efficiency of the MVHR. Higher inlet air temperature to the MVHR decreases its heat recovery efficiency. As discussed in both papers, unnecessary high inlet temperature only increased the exhaust air temperature leaving the building. In other words, a large amount of the recovered heat in that case would be simply just bypassed to the outdoor environment. Equation 3.1 represents the temperature transfer efficiency of an MVHR system. It shows how an increase in exhaust temperature leads to lower temperature transfer efficiency of MVHR. Therefore, by using an air preheater in front of an existing (in series with) MVHR, the temperature efficiency of the heat exchanger in MVHR will drop, resulting in an unnecessary energy loss.

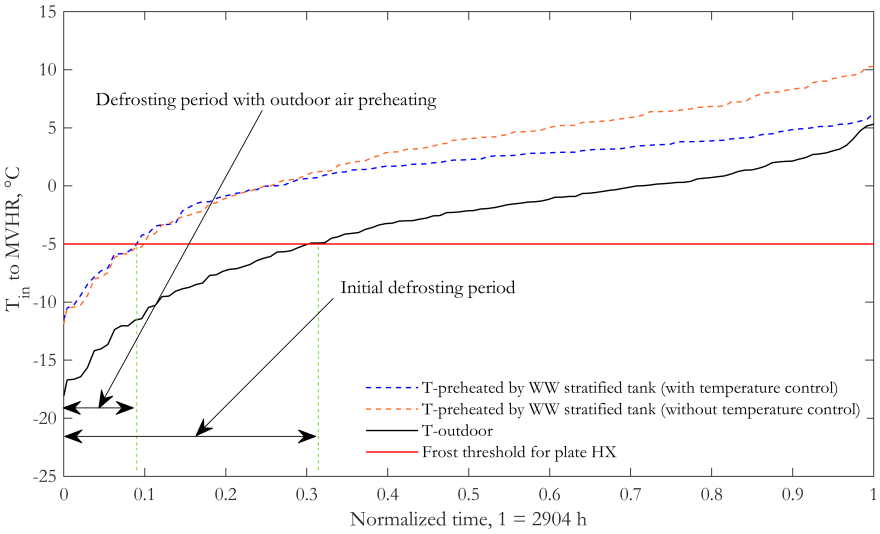

Figure 3.4: Reduction of defrosting need of MVHR by outdoor air preheating systems without and with temperature control (Nourozi et al., 2019)

$$\eta_{MVHR} = \frac{T_{supply} - T_{outdoor}}{T_{return} - T_{outdoor}} \tag{3.1}$$

Figure 3.5 depicts how an unnecessary increase in outdoor air temperature above the frost threshold can affect the temperature efficiency of the heat exchanger at MVHR. According to Equation 3.1, by maintaining supply and return temperatures constant, the decrease in efficiency results in higher exhaust air temperature, as shown in Figure 3.5a. This means that air with higher temperature that transfers more thermal energy is directed to outdoor; see Figure 3.5c.

In Papers 2, 6, and 7, three outdoor air preheating systems were compared from two different perspectives; one was the potential of each system in utilizing renewable heat sources to increase the outdoor air temperature above the frost threshold, and the second was the evaluation of the cost effectiveness of each system for a 20-year period. Geothermal energy as an available renewable heat source (System 1) and the residential wastewater stored in two types of storage tanks were compared in detail: a stratified storage tank, which was denoted as System 2, and an unstratified storage tank, which was identified as System 3.

Figure 3.6 illustrates the heat recovery potential of the three air preheating systems and the required energy for the circulation pumps. System 1, the air preheater using

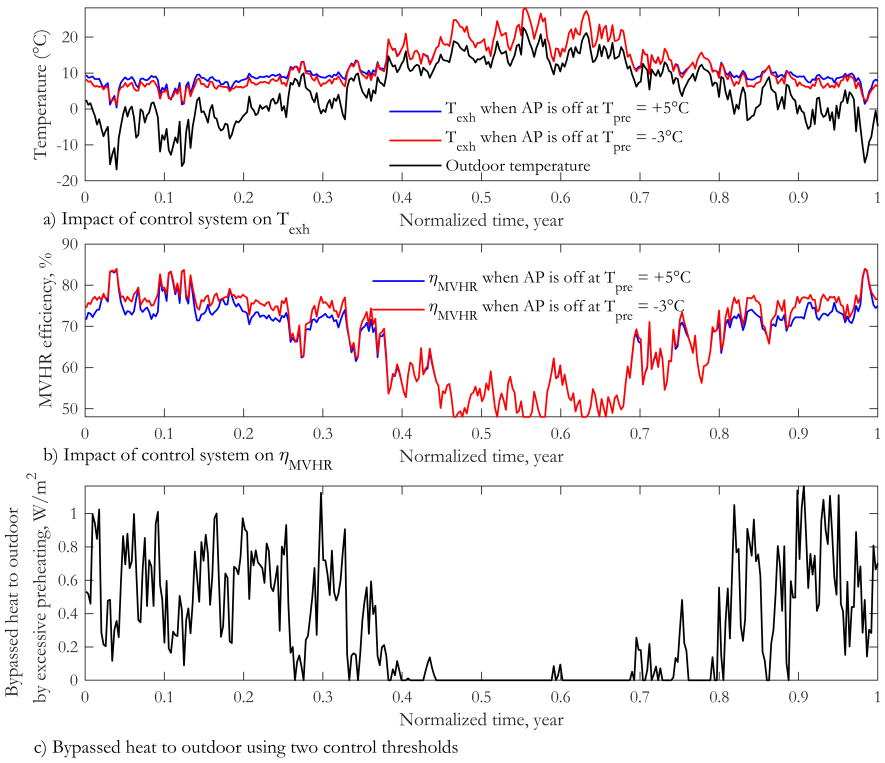

Figure 3.5: The effect of preheating outdoor air above threshold on exhaust air, MVHR temperature efficiency, and bypassed energy

geothermal energy as the heat source, required noticeably higher pumping power compared to the wastewater air preheaters. This was mainly due to the circulation of brine in the borehole's U-pipe heat exchanger. However, the transmitted heat rate to the outdoor air by System 1 was similar to System 3 and lower than System 2; see Figure 3.6b.

Figure 3.7 shows the accumulative initial and operational costs of each system compared to the base case in a 20-year period. The payback time for each system can be identified at the points where each system curve interacts with the base case. It can be seen that System 3 had the shortest payback time, approximately eight years. This was mainly due to minor electricity requirements for the circulation pump and lower initial investments since the unstratified tank was much cheaper than the stratified tank and drilling a borehole. A break-even point for System 2 was reached at about 17 years. Although the average increase in accumulated costs

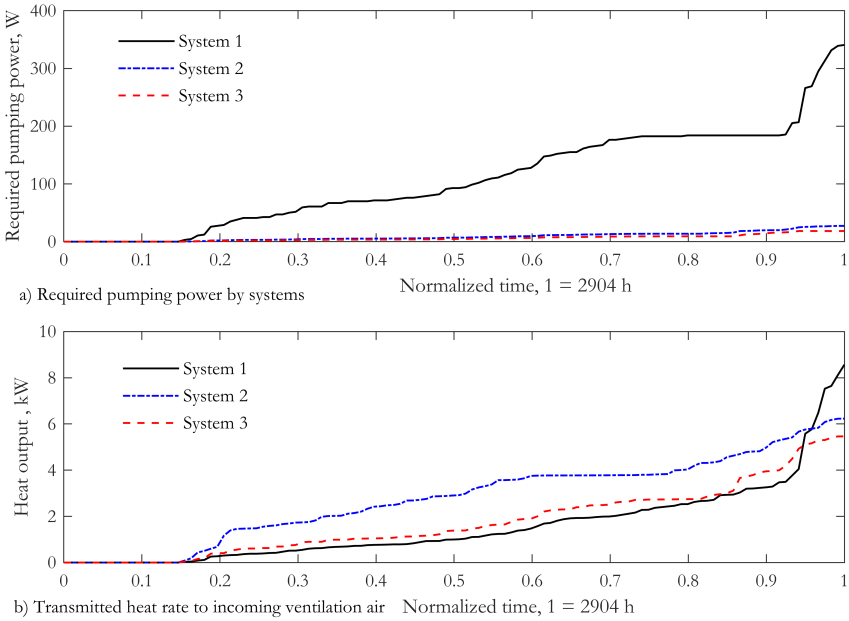

Figure 3.6: Required pumping power and the output heat rate, 1 = 2904 h (Nourozi et al., 2019)

for all air preheating systems was 13 000 SEK/year, the benefits from System 1 could not break even with the costs within the 20-year period. The initial costs for System 1, mainly drilling the borehole, were more than twice as those of the base system.

The tips and guidelines regarding outdoor air preheating in order for frost avoidance are presented in a flowchart in Figure 3.8. The outgoing grey water temperature from the building decreases from 19–25°C to 5–7°C by wastewater heat recovery. This recovered thermal energy is utilized for increasing the incoming outdoor air temperature to MVHR. If preheated air temperature is above the frost threshold, the temperature efficiency of MVHR drops significantly, which results in higher exhaust air temperature. Therefore, the recovered heat from wastewater would be bypassed and not saved in the system.

The highest possible temperature efficiency of MVHR is accomplished by preheating the incoming ventilation air just to above frost threshold. This provides the closest supply and return air temperatures, increases the heat recovery efficiency, and avoids frosting in the heat exchanger. The exhaust air temperature in this case

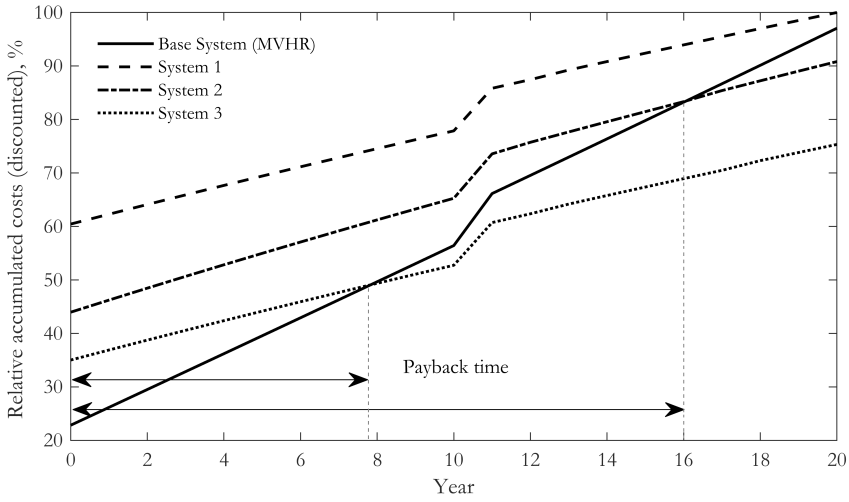

Figure 3.7: Accumulated cost and discounted payback period of the studied systems (Härer, 2019)

increases just to a point that ensures a heat exchanger surface temperature on the cold side above 0°C to avoid the internal frost formation. Thus, the lowest possible amount of the recovered heat energy from wastewater is bypassed to the outdoor air.

As the present study has shown, preheating the cold outdoor air can reduce or eliminate the defrosting need of MVHR; however, this approach will further decrease the relative humidity of the supply air to the building. The low relative humidity of the preheated air is not suitable in terms of indoor air quality and health issues. This topic was beyond the scope of current research work, but could be investigated further.

3.2 Condensation and frosting in ventilation heat exchanger

Paper 3 presented simulation results regarding a ventilation heat exchanger during the winter season. Various working conditions were investigated and the most important findings are summarized in this section. More detailed results are available in Paper 3.

Figure 3.9 illustrates air and plate temperature variation in the heat exchanger for two cases of dry and condensation flow conditions of the return air stream. In both cases, the return air temperature was 22°C, with a relative humidity of 30% and the outdoor air relative humidity was 85%. At the outdoor temperature of 0°C, the

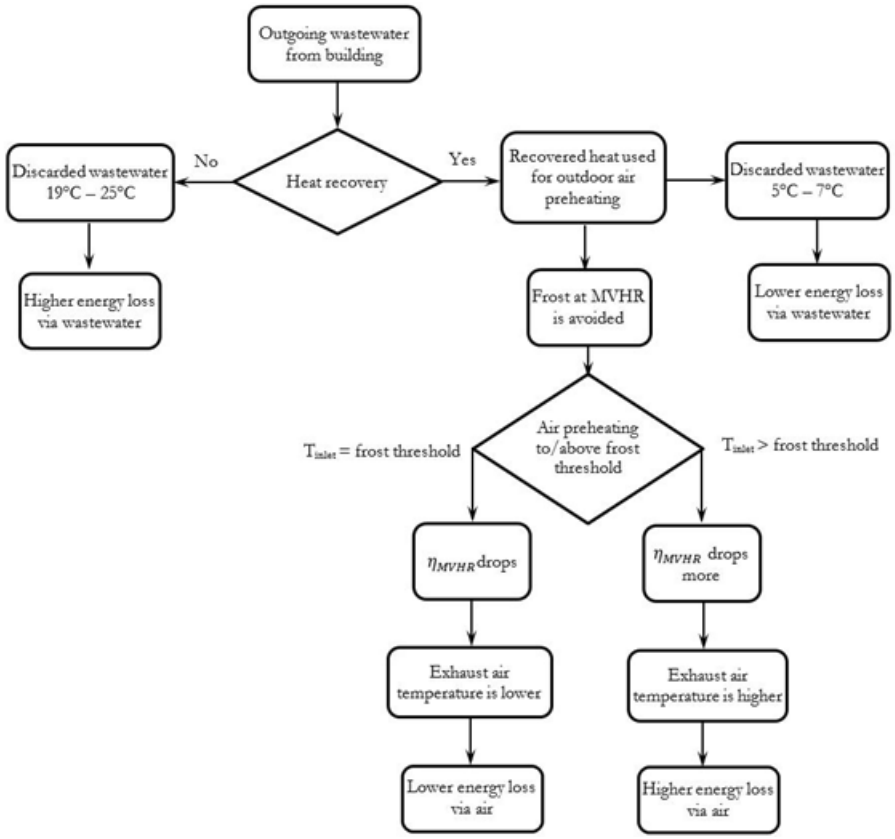

Figure 3.8: Energy flow and the impact of preheated temperature control on energy saving

entire span of the heat exchanger was in dry condition. The relative humidity in the return air stream increased to 100% at the exit, which shows that condensation did not occur before the air left the heat exchanger. The supply outdoor air temperature increased from 0°C to 16.6°C, and the relative humidity dropped to 28%. Figure 3.9 presents balanced supply and return ventilation flows. Therefore, the heat transfer rate and the convective heat transfer coefficients between the air streams and the plate were approximately equal, which made the plate temperature almost the average of the supply and return air temperatures.

At the lower outdoor temperature of -3°C, condensation occurred in the warm air stream before the air left the heat exchanger. Figure 3.9b shows that 17% of the heat exchanger length was exposed to condensation where there is a step-change in the plate temperature. A more significant heat transfer rate from the return

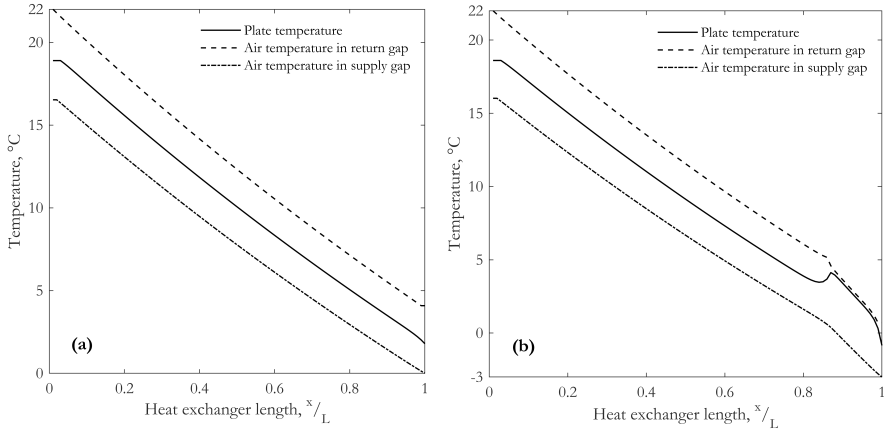

Figure 3.9: Temperature variation in the investigated heat exchanger – Dry vs. condensation

air stream to the plate caused an increased plate temperature. A slight rise in the supply temperature to the building is also observed. Because of condensation, this is less significant than the temperature change in the return stream. It is noteworthy that the plate temperature at the end of the heat exchanger falls below 0°C. This means that, in order to prevent frost formation in the heat exchanger, the incoming outdoor air temperature should be heated to above -3°C if the average relative humidity of the return air to the air handling unit is 30%.

Prescribed imbalanced airflow rates in supply and return ducts can be used to manipulate the thermal capacity of the air streams. Increasing the airflow rate of the return air stream was expected to contribute to postponing the frost threshold. This is investigated and shown in Figure 3.10.

Figure 3.10 illustrates temperature variation in a heat exchanger with balanced airflow rates compared to three imbalanced cases. Plate temperature is the lowest (dotted line) compared to other cases if the return flow rate is lower than the supply. In this case, condensation occurred in the last 23% of the heat exchanger and there was a risk of frosting as the plate temperature was below 0°C before the air left the heat exchanger. In this case, the building was overpressured. The balanced flow rates maintained the plate temperature above 0°C for the entire heat exchanger length. Increasing the return airflow rate and maintaining a constant supply flow rate resulted in a rise in the plate temperature. In this case, the condensation region shrank, thereby the risk of frost formation did too.

Flow properties in the heat exchanger are mainly a function of the design and can

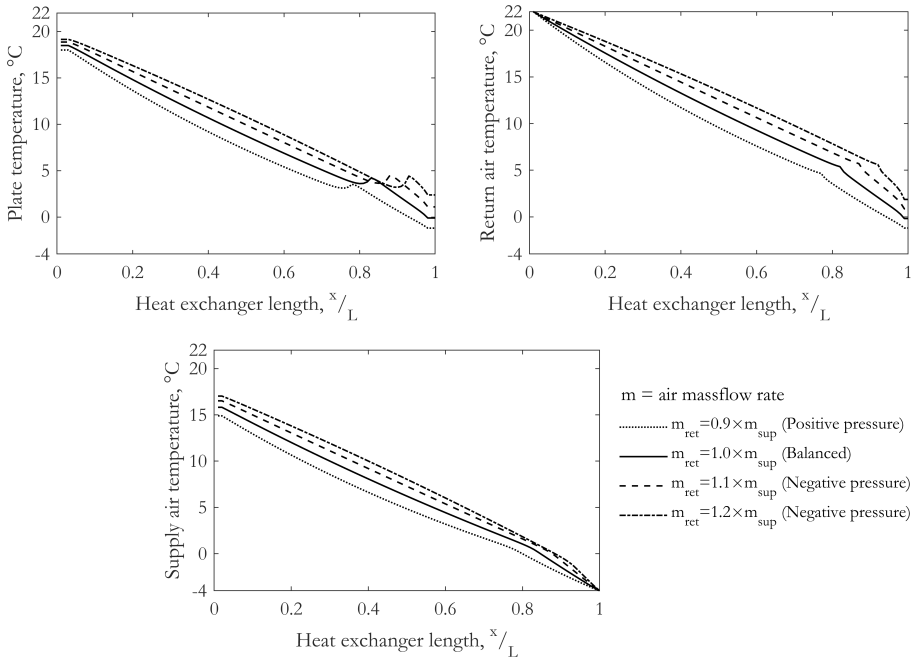

Figure 3.10: Effect of airflow imbalance on the condensation point and temperatures in the heat exchanger, $T_{ret} = 22°C$, $RH_{ret} = 30\%$ and $T_{out} = -4°C$

vary with the distance between the heat exchanger plates. Considering the assumption of evenly distributed air to the small gaps between the plates, changing the plate distance will affect characteristic length in calculating heat transfer coefficients. Figure 3.11 depicts the influence of the plate distance on the plate and air temperatures and the condensation point.

As shown in Figure 3.11, the condensation point moves towards the end of the heat exchanger with the increase in the slot size, which indicates the diminution of the condensation period. Firstly, this is attributed to reduced heat transfer rates due to a lower Reynolds number in wider air passages. Secondly, in the case of wider slots, the number of plates is reduced and the total heat transfer area of the heat exchanger. This significantly reduces the heat transfer rate of the exchanger and results in a lower supply air temperature. Also, the operation condition changes from wet to dry for wider slots as the plate temperature increases at the outdoor side. However, the supply temperature to the apartments reduces due to a lower surface temperature at the indoor side.

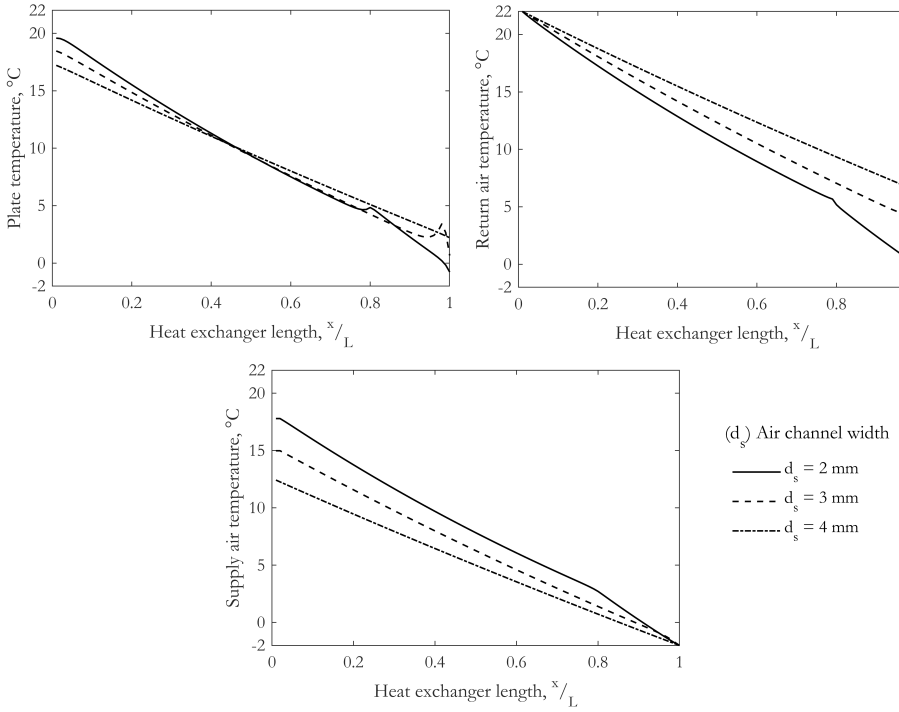

Figure 3.11: Effect of slot size on the condensation point and temperatures in the heat exchanger, $T_{ret} = 22°C$, $RH_{ret} = 30\%$ and $T_{out} = -2°C$

Figure 3.12 shows the impact of prescribed flow imbalance on the frost threshold for an indoor air relative humidity range of 25-40%. The results presented in Figure 3.12a are for a heat exchanger with a 2mm-distance between the plates, and Figure 3.12b is for a 3mm plate distance. Increasing the flow imbalance ratio (return-to-supply) from 0.9 to 1.1 resulted in the frost threshold rising in both heat exchangers with different plate distancing, but this impact is more significant for the heat exchanger with the 3mm plate distance shown in Figure 3.12b.

It is noteworthy that, for indoor relative humidity of 25%, in both heat exchangers, the frost threshold is lower for a higher return air temperature (22°C). This is because, in the case of return air at 20°C and relative humidity of 25%, the dew point temperature is below 0°C, but for a return temperature of 22°C, the dew point temperature is above 0°C.

In general, it can be observed that the frost threshold for the heat exchanger with

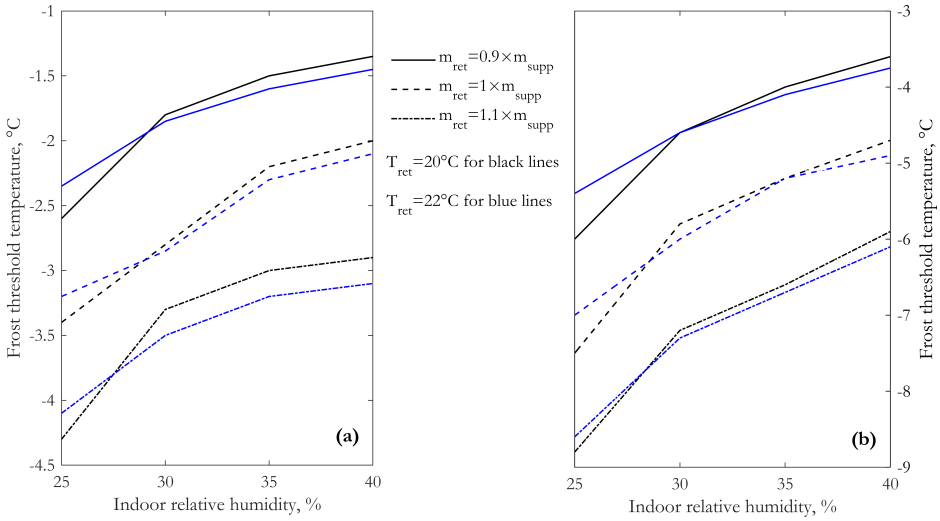

Figure 3.12: Effect of flow imbalance and return air temperature on frost threshold

3mm plate distance was lower than it was for the other case. By increasing the indoor air relative humidity, the frost threshold also increased in both cases since condensation occurred earlier. Indoor air temperature had a negligible impact on the frost threshold compared to indoor air relative humidity, airflow imbalance rate, and the heat exchanger design.

3.3 Energy active window (EAW)

Figure 3.13 depicts the air and pane temperature distribution along the EAW height. The indoor and outdoor temperatures were 20°C and -20°C, respectively, as introduced in Section 2. Supply air temperature to the slot was 20°C and the return air temperature at the bottom of window, as can be seen, was -5°C.

The supply and return air temperature in the slots was shown in Figure 3.13a. The air temperature at the upper part of the window was 14°C and it decreased to -5°C at the bottom of the return slot where it left the window. The glass temperatures shown in Figure 3.13b, T_1, T_3, T_4, and T_6 comply with the surface temperatures presented in Figure 2.10. Surface temperatures T4 and T6 were almost constant along with the window height compared to the other two (T_1 and T_3). The representative U-value, along with the window height, was shown in Figure 3.13c. The indoor heat transfer coefficient, h_{in}, varied from 6.8–7.1 W/m^2K, and the U-value varied from 0.5–0.7 W/m^2K. This is due to different inner glazing temperatures and indoor heat transfer coefficients (Nourozi et al., 2020).

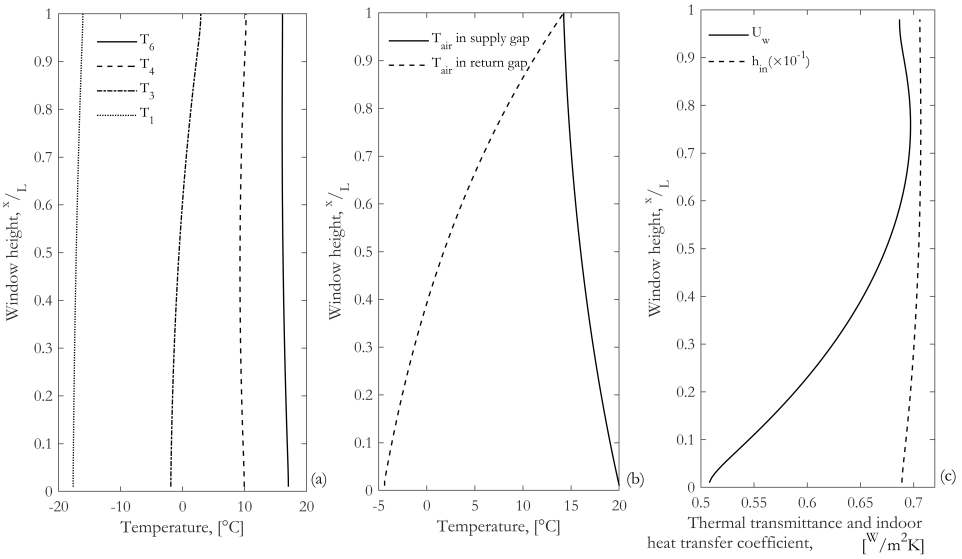

Figure 3.13: Air and panes temperature and U-value along the height of the EAW

Figure 3.14 shows the impact of slots size of the EAW on the U-value, along with the window height and the return air temperature from the window. Three cases of slot width of 10mm, 12.5mm, and 15mm in a range of 15-35°C injected air temperatures were simulated. By increasing the slot size, the return air temperature also increased. In contrast, the average U-value along the window height decreased when supply temperatures were raised. However, at a supply air temperature of approximately 18°C, the effect of slot size on the U-value was negligible. Therefore, the U-value decreased in wider slots and for supply air temperatures below 18°C, and increased for wider slots and for supply air temperatures above 18°C (Nourozi et al., 2020).

Window manufacturers commonly define windows U-values for a specific temperature difference on the two sides of the window surfaces. In practice, since the outdoor temperature changes, the temperature difference at the two sides of the window vary as well. Figure 3.15 indicates the influence of outdoor temperature on the U-value and the return air temperature from the EAW slots. The obtained results are presented for four different supply air temperatures to the slots. Note that the a constant indoor temperature of 20°C was used for the entire simulations. Thus, the temperature difference at the two sides of the window ranged from 10-50°C.

As can be seen in Figure 3.15, a constant rise in the return air temperature is

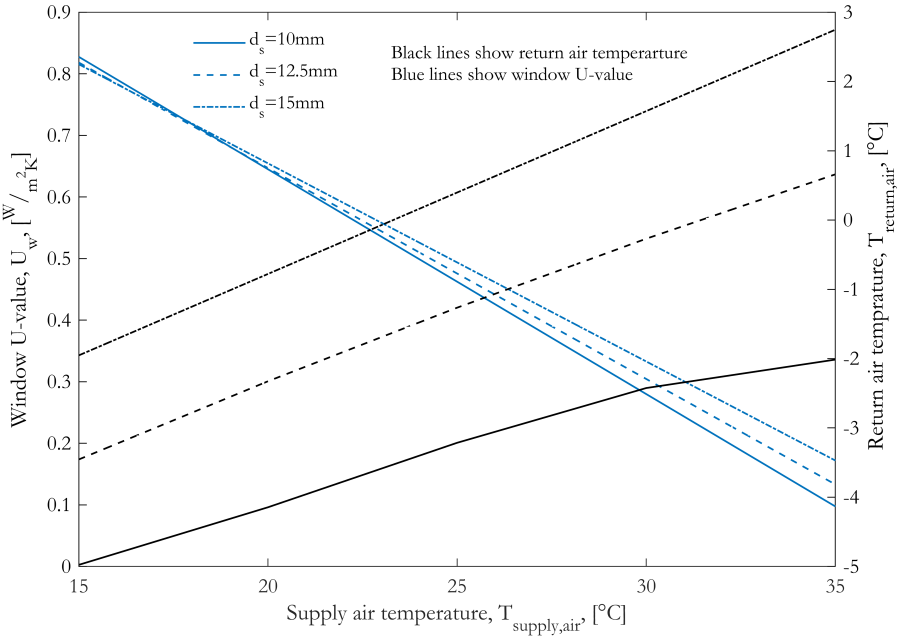

Figure 3.14: Impact of slot size on air temperature in the slots and U-value

observed by increasing the outdoor temperature, which was not affected by the supply air temperature. However, the supply air temperature impacted the average U-value of the window along the height. The U-value increased by increasing the outdoor temperature, for supply air temperatures below 20°C. This trend was different for supply air temperatures above 20°C, as the U-value decreased with increasing outdoor temperature (Nourozi et al., 2020).

The latest Swedish building regulation release provided by Boverket (The Swedish National Board of Housing, Building and Planning) mandates a window glazing area of at least equal to 10% of the floor area (Boverket, 2019). The investigated energy active window in this research work, presented in Figure 3.13, can be compared to a conventional window with a nominal U-value of 1.2 W/m^2řC at two outdoor temperatures of -20°C and -5°C, using Equation 3.2. The heat gains by replacing the conventional window with an EAW will be 13–22 W for each window unit area. Assuming a 10% window-to-floor area ratio and given the indoor/outdoor conditions, EAW can reduce the room heating demand by 1.3-2.2 $W/m^2_{floorarea}$ for the mentioned outdoor temperatures.

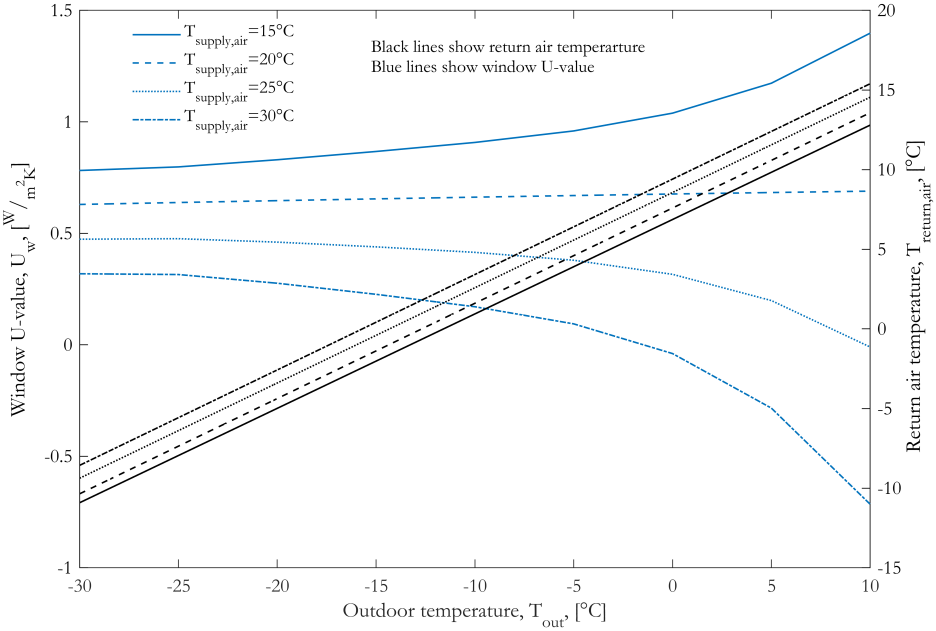

Figure 3.15: Impact of outdoor temperature on EAW U-value, $T_{in} = 20°C$

$$\frac{Q_{gain}}{A_{floor}} = (U_{TGW} - U_{EAW})(T_{in} - T_{out})\frac{A_w}{A_{floor}} \tag{3.2}$$

Chapter 4

Practical implications

Geographical impact on indoor air relative humidity is an important aspect when considering outdoor air preheating. In north Sweden, air humidity is low compared to southern and central parts of Sweden and will decrease even more by preheating the air before the air handling unit. This will introduce dry air to the building. It is shown by Sterling et al. (1985) that in dry air conditions, the likelihood of respiratory infection increases, and the perceived indoor air quality decreases. Sterling et al. have also demonstrated that the risk of sustaining environments, where the growth of viruses, bacteria, molds, mites, and some insects is facilitated, is higher in environments where the relative humidity is not within a prescribed range of 30%-60%.

Previous investigations, listed in Table 1, provided guidelines for identifying the frost threshold for specific prevalent indoor and outdoor conditions. Most installed cases follow recommendations based on pressure drop control over the heat exchanger by lifting the air temperature above a static temperature threshold to avoid heat exchanger frosting. However, active monitoring of the critical parameters in defining the frost threshold is suggested in this study. Realtime monitoring of return air relative humidity, outdoor air temperature, airflow imbalance rate, and considering the heat exchanger design specifications can lead to correct anticipation of frost threshold. Currently, air humidity is not measured in Swedish residential buildings, and this is a limiting factor for pro-active anticipation of freezing start in the heat exchanger. It is noteworthy that the placement of - humidity sensors should be at the air handling unit entrance for return air to precisely evaluate the frost threshold.

Building type can also affect the indoor air condition and, in turn, impact the frost threshold at the air handling unit. In buildings with dense occupants and relatively small living space per person, such as student dormitories, the relative humidity in the return air from the apartments is more humid compared to the other residential buildings. This affects the frost threshold in the air handling unit. A shared large laundry room placed in a building and its operating time will also cause highly moist air to the AHU, which in turn will enhance the risk of freezing in the heat exchanger.

In Paper 3, it was shown that condensation improves heat transfer between the air streams and is favorable for increasing the supply air temperature to the building.

However, when condensation occurs in the heat exchanger, a layer of liquid forms on the surface and occupies the small distance between the plates ($\approx 2-3mm$). This increases the air pressure loss over the heat exchanger and might trigger the defrosting mode, decreasing the thermal efficiency.

In this research work, airflow imbalance is analyzed as an alternative solution to avoid/postpone frost formation in the heat exchanger. In fact, a higher return airflow rate than the supply provides potential possibility for increasing the plate temperature to above the frost threshold. This airflow imbalance causes a negative pressure that could affect door/window opening in the building if excessively exaggerated. Furthermore, a negative indoor pressure due to flow imbalance of approximately 10% is common for clean outdoor air, which is the case in Scandinavia. However, positive indoor pressure is recommended to limit unwanted infiltration in countries with polluted outdoor air.

In Paper 1, it was discussed that a high heat recovery efficiency results in low extract air and plate temperatures. This increases the chance of frosting in the heat exchanger. However, the heat recovery efficiency of the heat exchanger drops over time, decreasing the chance of frost formation. Indeed, the frost thresholds suggested by TRNSYS (Paper 5) and Matlab simulations (Paper 3) differed in our studies. Therefore, considering an uncertainty band in anticipating the exact frosting temperature in the heat exchanger is inevitable.

Preventing frost formation in heat exchangers considerably decreases the heat load demand of buildings during cold periods. At the same time, the supply air temperature to the buildings is as essential in reducing buildings' load demand, which has not been discussed much in this research work. Detecting the frost threshold ensures a frost-free operation in the heat exchanger, while higher inlet air temperatures may impact the supply air temperature to the building and diminish the need for air post-heating. Therefore, there is a trade-off between reduction in heat recovery efficiency of the air handling unit by excessive air preheating and increasing the supply air temperature to the building to the desired level.

Chapter 5

Concluding remarks and future work

5.1 Conclusion

This doctoral thesis presented a summary of the entire research work on the waste heat recovery potential in residential buildings and the use of renewables to reduce the peak heating load of these buildings during cold winter periods. Frosting, a common problem in mechanical ventilation systems with heat recovery in cold climates, has been investigated. Residential wastewater and local geothermal energy are the two sources used for outdoor air preheating to eliminate frosting in mechanical ventilation systems. A detailed study on the performance of ventilation heat exchangers was conducted and technical guidelines for implementation have been provided. Contributions from a novel window type to improve the thermal performance of the building have also been investigated. Based on the presented results in this thesis and the appended papers, the following conclusions are drawn:

The efficiency of the heat exchanger in MVHR is a decisive factor for frost formation. A high heat exchanger efficiency provides a supply temperature close to room temperature. This, in turn, requires a high cooling of the return air, resulting in excessive condensation and possibly frost growth in the heat exchanger. Therefore, by preheating the inlet air to MVHR, the heat exchanger's efficiency decreases, resulting in higher exhaust air temperature and, subsequently, heat exchanger surface temperature, thereby preventing frost formation.

Utilizing an appropriate control system to preheat the incoming outdoor air to just above the frost threshold will ensure the highest possible heat exchanger efficiency at MVHR and decrease the operation time of the wastewater or brine circulation pump. Therefore, identifying a "correct" frosting limit is crucial for an efficient operation. Outdoor air preheating systems using heat from the stored wastewater have a higher probability of generating savings within the 20-year operation period. Break-even time for the systems utilizing wastewater was reached after 8 and 17 years (for unstratified and stratified tanks, respectively). However, geothermal energy exploitation requires higher initial investment and operational costs, making the payback period longer than 20 years.

In the ventilation heat exchanger, condensation caused a sharp increase in the plate

temperature where the heat transfer rate between the return airflow and the plate increased greatly. However, the convective heat transfer between the supply airflow and the plate increased slightly. Therefore, the supply air temperature to the rooms was lifted slightly and was approximately the same as in dry operation.

The return air relative humidity was another decisive parameter that influenced the frost threshold. Installation of a relative humidity sensor at the inlet of the heat exchanger would contribute to a more precise prediction of the condensation/frost onsets. The control system would effectively utilize the frosting limit data to enable imbalanced airflows in supply and return ducts or preheat the outdoor air using a geothermal source to prevent/delay frost formation in the heat exchanger.

The thermal performance of the energy-active window (EAW) is significantly influenced by supply (injected) air temperature variations, as also seen in MVHR systems. Low U-values ($< 0.65\ W/m^{2\circ}C$) are obtained if the supply air temperature to EAW was above the indoor temperature. At outdoor temperatures of -20°C and -5°C, and a building with a window-to-floor area ratio of 10%, the EAW could potentially reduce the heating load demand by approximately 2.2 $W/m^2_{floorarea}$ and 1.3 $W/m^2_{floorarea}$, respectively. This potential increases proportionally with the window-to-floor area ratio. It was also observed that the initial energy performance of windows is a decisive parameter for achieving additional energy savings with EAW. The higher the initial efficiency, the lower the potential for additional performance improvements. This was also observed for MVHR systems, as elaborated above.

5.2 Future work

The primary goal of this doctoral work was to develop methods to decrease the peak heating loads of residential buildings during cold winter days. The focus was on shaving the heating load of the air handling unit when frosting occurs. The frosting conditions were identified and methods to prevent frosting were suggested. However, the need for air post-heating can be a further investigation. In cases of low outdoor temperature, using the suggested approaches can ensure a frost-free operation of a plate heat exchanger. Still, the supply air temperature to the building could not reach the desired setpoint temperature ($\approx 18^{\circ}C$). Considering the availability of the preheating resources, future investigations could aim to identify an optimum air preheating temperature that prevents frost formation in the heat exchanger and lifts the supply air temperature close to the setpoint.

Further investigations on the life cycle analysis (LCA) of the suggested air preheating systems will provide a comparison between the environmental impacts of utilizing air preheating systems' components such as boreholes, wastewater tanks, pumps, distribution pipes, and the energy/power saved by the outdoor air pre-

heating. Together with the cost-saving benefits of the investigated systems, these results would further clarify the practical feasibility of the suggested air preheaters.

References

Anisimov, S., A. Jedlikowski, and D. Pandelidis (2015). Frost formation in the cross-flow plate heat exchanger for energy recovery. *International Journal of Heat and Mass Transfer 90*, 201–217.

Bar-Cohen, A. and W. Rohsenow (1984). Thermally optimum spacing of vertical, natural convection cooled, parallel plates.

BBR (2018). Mandatory provisions and general recommendations.

Bergman (2009). *Double column windows, Test of function and performance (Dubbelspaltfönster Test av funktion och prestanda)*. Ph. D. thesis, Uppsala Univeristy.

Bergman, T. L., A. S. Lavine, F. P. Incropera, and D. P. DeWitt (2017). *Incropera's principles of heat and mass transfer*. Wiley Global Education.

Boverket (2019). Boverket´ s mandatory provisions and general recommendations, bbr, bfs 2011: 6 with amendments up to bfs 2018: 4.

Cengel, Y. A. and A. J. Ghajar (2014). *Heat and mass transfer: fundamentals and applications*. McGraw-Hill Higher Education.

Churchill, S. W. and H. H. Chu (1975). Correlating equations for laminar and turbulent free convection from a vertical plate. *International journal of heat and mass transfer 18*(11), 1323–1329.

EU Directive 2018/2001 (2018). 2001 of the european parliament and of the council of 11 december 2018 on the promotion of the use of energy from renewable sources. *European Commission: Brussels, Belgium*.

EU Directive 2018/2002 (2018). Directive (eu) 2018/2002 of the european parliament and of the council of 11 december 2018 amending directive 2012/27. *EU on energy efficiency*.

(EU) No 244/2012 (2012). Guidelines accompanying commission delegated regulation (eu), no. 244/2012 of 16 january 2012 supplementing directive 2010/31/eu of the european parliament and of the council on the energy performance of buildings by establishing a comparative methodology framework for calculating cost-optimal levels of minimum energy performance requirements forbuildings and building elements. *Official Journal of the European Union 55*, 1–28.

Fisk, W., R. Chant, K. Archer, D. Hekmat, F. Offermann, and B. Pedersen (1985). Onset of freezing in residential air-to-air heat exchangers. *ASHRAE transactions 91*(1), 145–158.

Fisk, W. J., K. M. Archer, R. E. Chant, D. Hekmat, F. Offermann, and B. S. Pedersen (1983). Freezing in residential air-to-air heat exchangers: an experimental study. Technical report, Lawrence Berkeley National Lab.(LBNL), Berkeley, CA (United States).

Grahn, E. (2019). Energy in sweden: Facts and figures 2019.

Härer, S. (2019). *Life Cycle Cost Analysis of novel Heat Recovery Systems using renewable Heat Sources*. Ph. D. thesis, KTH Royal Institute of Technology.

Hesselgreaves, J. E., R. Law, and D. Reay (2016). *Compact heat exchangers: selection, design and operation*. Butterworth-Heinemann.

Huber, H. Hydropress huber ab- waste water solutions.

Huber, H. (2019). Imbalance and temperature ratio of non- ducted mechanical supply and exhaust ventilation units - results of a swiss field investigation and calculation of the impact of imbalance to the temperature ratio. Technical report, Lucerne University of Applied Sciences and Arts.

Kempe, P. and R. Jonsson (2015). Nybyggt flerbostadshus med förvärmning med borrhålsvatten-hsb-ftx geoenergi utan värmepump (newly built apartment buildings with air preheating using borehole water-hsb balanced ventilation with heat recovery served by geothermal energy without heat pumps). *BeBo (Swedish Energy Agency network for energy-efficient apartment buildings)*.

Kragh, J., J. Rose, T. R. Nielsen, and S. Svendsen (2007). New counter flow heat exchanger designed for ventilation systems in cold climates. *Energy and Buildings 39*(11), 1151–1158.

Larsson, U., B. Moshfegh, and M. Sandberg (1999). Thermal analysis of super insulated windows (numerical and experimental investigations). *Energy and Buildings 29*(2), 121–128.

Le Truong, N., A. Dodoo, and L. Gustavsson (2014). Effects of heat and electricity saving measures in district-heated multistory residential buildings. *Applied Energy 118*, 57–67.

Levin, P. and C. Karlsson (2015). One house, five possibilities - demonstration project for energy efficiency in existing multi-dwelling buildings from the million program time (demonstrationsprojekt för energieffektivisering i befintliga flerbostadshus).

Meggers, Forrest, L.-H. (2011). The potential of wastewater heat and exergy: Decentralized high-temperature recovery with a heat pump. *Energy and Buildings 43*(4), 879–886.

Meteonorm. Meteonorm, https://meteonorm.com/en/.

Nasr, M. R., M. Fauchoux, R. W. Besant, and C. J. Simonson (2014). A review of frosting in air-to-air energy exchangers. *Renewable and Sustainable Energy Reviews 30*, 538–554.

Nasr, M. R., M. Kassai, G. Ge, and C. J. Simonson (2015). Evaluation of defrosting methods for air-to-air heat/energy exchangers on energy consumption of ventilation. *Applied Energy 151*, 32–40.

Nourozi, B., A. Ploskić, Y. Chen, J. N.-W. Chiu, and Q. Wang (2020). Heat transfer model for energy-active windows–an evaluation of efficient reuse of waste heat in buildings. *Renewable energy 162*, 2318–2329.

Nourozi, B., Q. Wang, and A. Ploskić (2019). Energy and defrosting contributions of preheating cold supply air in buildings with balanced ventilation. *Applied Thermal Engineering 146*, 180–189.

Nourozi, B., Q. Wang, and A. Ploskic (2019). Identifying frost threshold in a balanced mechanical ventilation system by inlet and exhaust air temperature control. In *The 11th International Symposium on Heating, Ventilation and Air Conditioning (ISHVAC2019)*.

Nourozi, B., Q. Wang, and A. Ploskić (2019). Maximizing thermal performance of building ventilation using geothermal and wastewater heat. *Resources, Conservation and Recycling 143*, 90–98.

Orpana, L. (2016). Air treatment system in energy calculations a study of product data and calculation methods(luftbehandlingssystem i energiberäkningar en studie av produktdata och beräkningsmetoder). *SBUF (Development Fund of the Swedish Construction Industry)*.

Pacak, A., A. Jedlikowski, M. Karpuk, and S. Anisimov (2019). Analysis of power demand calculation for freeze prevention methods of counter-flow heat exchangers used in energy recovery from exhaust air. *International Journal of Heat and Mass Transfer 133*, 842–860.

Papanicolaou, E. and Y. Jaluria (1991). Mixed convection from an isolated heat source in a rectangular enclosure. *Numerical Heat Transfer 18*(4), 427–461.

Ploskić, A. and Q. Wang (2018). Evaluating the potential of reducing peak heating load of a multi-family house using novel heat recovery system. *Applied Thermal Engineering 130*, 1182–1190.

Raji, A. and M. Hasnaoui (1998). Mixed convection heat transfer in a rectangular cavity ventilated and heated from the side. *Numerical Heat Transfer, Part A Applications 33*(5), 533–548.

Shah, R. K. and A. L. London (2014). *Laminar flow forced convection in ducts: a source book for compact heat exchanger analytical data*. Academic press.

SHARC. Sharc energy systems, http://www.sharcenergy.com/.

Simanic, B. (2016). Förvärmning av ventilationsluft mha borrhålsvärme utan värmepump, fallstudie vivalla örebro. *Tekn. rapport. Svenska byggbranschens utvecklingsfond*.

Singh, S. and M. Sharif (2003). Mixed convective cooling of a rectangular cavity with inlet and exit openings on differentially heated side walls. *Numerical Heat Transfer: Part A: Applications 44*(3), 233–253.

Song, M. and C. Dang (2018). Review on the measurement and calculation of frost characteristics. *International Journal of Heat and Mass Transfer 124*, 586–614.

Statens Energimyndighet (2016). ummary of energy statistics for dwellings and non-residential premises for 2016 (energistatistik för småhus, flerbostadshus och lokaler 2016). *Energy statistics for one family houses, multifamily houses and premises*.

Sterling, E., A. Arundel, and T. Sterling (1985). Criteria for human exposure to humidity in occupied buildings. *ASHRAE transactions 91*(1), 611–622.

Sundin, M. (2018). Geothermal preheating of ventilation air: An evaluation of the ventilation efficiency of the ventilation system (geotermisk förvärmning av ventilationsluft: En utvärdering av ventilationssystemets energieffektivitet).

Swedish Energy Agency (2017). Energy in sweden 2017.

TRNSYS. Trnsys: Transient system simulation tool.

Vattenfall (2019). District heating prices (fjärrvärmepriser).

Wang, Z.-Z. and Z.-N. Zhao (1993). Analysis of performance of steam condensation heat transfer and pressure drop in plate condensers. *Heat Transfer Engineering 14*(4), 32–41.

Weather in Stockholm. Weather in stockholm. swedish meteorological and hydrological institute.

Appendix: Papers